Development of a human liver microphysiological coculture system for higher throughput chemical safety assessment

Toxicological sciences

Ip, Blanche C.; Madnick, Samantha J.; Zheng, Sophia; van Tongeren, Tessa C.A.; Hall, Susan J. et al

https://doi.org/10.1093/toxsci/kfae018

OXFORD
SOT | Society of Toxicology
academic.oup.com/toxsci

Toxicological Sciences, 2024, 1–19
https://doi.org/10.1093/toxsci/kfae018
Advance Access Publication Date: February 9, 2024
Research article

Development of a human liver microphysiological coculture system for higher throughput chemical safety assessment

Blanche C. Ip [1,2,*] Samantha J. Madnick,[1,2] Sophia Zheng,[1] Tessa C.A. van Tongeren [3] Susan J. Hall,[1] Hui Li,[1] Suzanne Martin,[4] Sandrine Spriggs,[4] Paul Carmichael,[4] Wei Chen,[5] David Ames,[5] Lori A. Breitweiser,[5] Heather E. Pence,[5] Andrew J. Bowling,[5] Kamin J. Johnson [5] Richard Cubberley,[4] Jeffrey R. Morgan,[1,2] Kim Boekelheide [1,2,*]

[1]Department of Pathology and Laboratory Medicine, Brown University, Providence, Rhode Island 02903, USA
[2]Center for Alternatives to Animals in Testing, Brown University, Providence, Rhode Island 02903, USA
[3]Division of Toxicology, Wageningen University and Research, 6700 EA Wageningen, The Netherlands
[4]Unilever, Safety and Environmental Assurance Centre, Colworth Science Park, Sharnbrook, MK44 1LQ Bedfordshire, United Kingdom
[5]Corteva, Inc, Indianapolis, Indiana 46268, USA

*To whom correspondence should be addressed at Department of Pathology and Laboratory Medicine, Brown University, Box G-E5, 70 Ship Street, Providence, RI 02903. E-mails: blanche_ip@brown.edu and kim_boekelheide@brown.edu.

Abstract

Chemicals in the systemic circulation can undergo hepatic xenobiotic metabolism, generate metabolites, and exhibit altered toxicity compared with their parent compounds. This article describes a 2-chamber liver-organ coculture model in a higher-throughput 96-well format for the determination of toxicity on target tissues in the presence of physiologically relevant human liver metabolism. This 2-chamber system is a hydrogel formed within each well consisting of a central well (target tissue) and an outer ring-shaped trough (human liver tissue). The target tissue chamber can be configured to accommodate a three-dimensional (3D) spheroid-shaped microtissue, or a 2-dimensional (2D) cell monolayer. Culture medium and compounds freely diffuse between the 2 chambers. Human-differentiated HepaRG liver cells are used to form the 3D human liver microtissues, which displayed robust protein expression of liver biomarkers (albumin, asialoglycoprotein receptor, Phase I cytochrome P450 [CYP3A4] enzyme, multidrug resistance-associated protein 2 transporter, and glycogen), and exhibited Phase I/II enzyme activities over the course of 17 days. Histological and ultrastructural analyses confirmed that the HepaRG microtissues presented a differentiated hepatocyte phenotype, including abundant mitochondria, endoplasmic reticulum, and bile canaliculi. Liver microtissue zonation characteristics could be easily modulated by maturation in different media supplements. Furthermore, our proof-of-concept study demonstrated the efficacy of this coculture model in evaluating testosterone-mediated androgen receptor responses in the presence of human liver metabolism. This liver-organ coculture system provides a practical, higher-throughput testing platform for metabolism-dependent bioactivity assessment of drugs/chemicals to better recapitulate the biological effects and potential toxicity of human exposures.

Keywords: liver metabolism; 3D coculture; toxicity testing; animal alternatives; *in vitro* testing; HepaRG.

Safety testing in the pharmaceutical, chemical, and consumer product industries is undergoing a transition from animal-based testing to human-derived cell models for *in vitro* testing. This transition is driven by 3 concurrent trends: (1) the development of more robust and predictive human *in vitro* models incorporating the techniques and capabilities discovered during the ongoing revolution in biology, (2) a growing recognition of the biological limitations inherent to using animals to predict human responses, and (3) increasing concern with the ethics of using animals as a surrogate test species for humans.

Substantial progress has been made in developing higher-throughput tests for *in vitro* toxicity and safety assessments of these products. These assays have mostly focused on the direct impact of tested compounds on tissues of interest. However, chemicals and drugs can circulate to the liver where they undergo xenobiotic metabolism and generate a spectrum of metabolites. Although generally acting to de-toxify chemicals, hepatic metabolism can generate metabolites that are more toxic than their precursors. *In vitro* approaches incorporating hepatic metabolism and target cells that measure cellular responses (eg, imaging, transcriptomics, activation of stress responses) could evaluate whether the biotransformation of a chemical would alter its toxicity, thus guiding its further characterization as a hazard.

The Alginate Immobilization of Metabolic Enzymes (AIME) platform was developed as an approach to retrofit existing high-throughput screening (HTS) assays with hepatic metabolic competence (Deisenroth *et al.*, 2020). The AIME system consists of 96-well microplate lids containing solid supports attached to alginate encapsulated rat hepatic S9 (hepatic microsomes and post-mitochondrial supernatant fractions), and this encapsulation minimizes S9-induced cytotoxicity (Bimboes and Greim, 1976; Cox *et al.*, 2016). These lids are then immersed in a medium with NADPH regeneration system (NRS) cocktails that support Phase I

xenobiotic metabolism, and has demonstrated the efficacy of including hepatic metabolism in enhancing the *in vivo* concordance of *in vitro* results with the rodent uterotrophic bioassay (Deisenroth *et al.*, 2020). However, the AIME platform presents a species-dependent cytochrome P450 profile (Ozawa *et al.*, 2000), and the utilization of S9 fractions fails to recapitulate the nonxenobiotic liver biology (chemical-protein binding, hepatic clearance, etc.) that can have crucial roles in the physiological impact of parent chemicals and their metabolites on extra-hepatic tissues. We need simple and rapid solutions to address the universal need to determine if a candidate drug or new chemical produces active metabolites in the presence of human liver metabolism, and that the biological impact of the active metabolite can be determined in a way that is compatible with predicting effects in humans.

Primary human hepatocytes (PHHs) are currently considered a "gold standard" for *in vitro* liver models, but their utility for chemical safety evaluation is severely limited by donor-specific variability, a finite supply from individual donors, and a rapid loss of hepatocyte functionality *in vitro* (Chao *et al.*, 2009; Godoy *et al.*, 2013; Jackson *et al.*, 2016; Mitaka, 1998; Nyberg *et al.*, 1994; Ozawa *et al.*, 2000; Parkinson, 1996). 3D human liver models using human hepatoma HepaRG cells (Gripon *et al.*, 2002) were shown to exhibit stable hallmarks of hepatocyte functionality lasting up to 60 days in some models (Gunness *et al.*, 2013; Hoekstra *et al.*, 2013; Jackson *et al.*, 2016; Leite *et al.*, 2012; Ramaiahgari *et al.*, 2017; Takahashi *et al.*, 2015; Yokoyama *et al.*, 2018), including (1) physiologically relevant drug metabolizing activities, (2) liver enzyme induction, and (3) evidence of biliary excretion functionality.

Our laboratory has previously developed an agarose hydrogel system that provides a stable environment for culturing cells as scaffold-free 3D microtissues with sustained physiological functions over time (Ip *et al.*, 2018, 2022; Leary *et al.*, 2018). In addition, the agarose hydrogel does not interfere with chemical concentration through chemical absorption (Ip *et al.*, 2022) unlike other biocompatible materials including the polymer polydimethylsiloxane (PDMS). PDMS, and similar materials used to build microfluidic devices compatible with cell culture (eg, "organ-on-a-chip"), tend to adsorb chemicals, altering drug response bioassays (van Meer *et al.*, 2017).

Here, we have described and executed a proof-of-concept study with our 2-chamber liver-organ coculture model in a higher-throughput 96-well format for the determination of toxicity on target tissues in the presence of physiologically relevant human liver metabolism. Importantly, this platform is designed to be scalable, so it can mimic the natural size differences between liver and other organs and produce sufficient quantities of metabolites to simulate the *in vivo* exposure setting. The overall goal is to develop and test a simple platform that incorporates human liver metabolism capable of perturbing a target tissue.

Materials and methods

Fabrication of 2-chamber coculture system in 96-well plate platform

Molds, designed using computer-assisted design (SolidWorks, Concord, Massachusetts), consisted of a base platform upon which lay a series of 6 rows by 8 columns of pegs, with each peg designed to fit within 1 well of a 96-well plate (ibidi, Gräfelfing, Germany) (Figure 1). Each of the pegs had 2 main components: a circular ring and a central peg that is either a conical-shaped micropost or a cylinder that touches the bottom of the well plate (Figure 1). To form hydrogels, a 2% weight/volume (w/v) molten agarose solution was made by dissolving sterile agarose (BP160-500; Fisher Scientific, Waltham, Massachusetts) in sterile phosphate-buffered saline (PBS) (Gibco 14190). Sterile 2% w/v molten agarose (135 µl) was pipetted into each well and the mold was placed on top of the plate with the circular ring and peg submerged in agarose. The molten agarose solution solidified in 8 min and the mold was removed. The resulting hydrogel that formed within each well contained an outer ring-shaped trough (human liver tissue chamber) with a central well (target tissue chamber) that is either a conical-shaped well to form a 3D spheroid-shaped microtissue, or a circular opening at the bottom of the plate to form a two-dimensional (2D) cell layer. The hydrogel was equilibrated with 200 µl of serum-free cell culture medium designed for selected cells supplemented with 1% penicillin/streptomycin for 24 h incubating at 37°C with 5% CO_2. The serum-free medium (William E supplemented with 1% Glutamax and 1% penicillin/streptomycin for HepaRG cells) was exchanged 2 more times with 24 h incubations in between prior to the seeding of cells.

Cell culture

Undifferentiated HepaRG (BioPredic International, Rennes, France) was thawed and maintained in HepaRG working growth medium consisting of Williams E medium supplemented with ADD711 HepaRG growth medium supplement, 1% GlutaMax (35050061, ThermoFisher), and 1% penicillin/streptomycin (Gibco 15140-122) per manufacturer's directions. Cells were maintained in an incubator at a temperature of 37°C at 5% CO_2.

Immortalized BHPrE (nontumorigenic human prostate epithelial cells) and BHPrS (benign human prostate stromal cells) cell lines were a gift from Simon Hayward and generated as described previously (Franco *et al.*, 2011). BHPrE is genetically labeled with red fluorescent protein (RFP), and BHPrS is genetically labeled with enhanced green fluorescent protein (EGFP). Both cell lines were maintained in DMEM/F-12 GlutaMAX (Gibco 10565-018; ThermoFisher) supplemented with 1% insulin-transferrin-selenium-sodium pyruvate (ITS-A, Gibco 51300044), 1% penicillin/streptomycin, 0.4% bovine pituitary extract (129-NZ-5, Cell Applications, San Diego, California), and 10 ng/ml epidermal growth factor. Medium was changed every 2–3 days. Cells were maintained in an incubator at a temperature of 37°C at 5% CO_2.

Culture of fluorescently labeled cells

Immortalized BHPrE-RFP and BHPrS-EGFP prostate cell lines were passaged as described previously (Franco *et al.*, 2011), and seeded at 50 000 cells/well into the ring trough. Cells were allowed to first settle by gravity into the bottom of the ring-shaped trough for 30 min, then 150 µl of prostate cell medium was added slowly into each of the wells without disturbing the prostate cells that have settled into the bottom of the ring-shaped trough. Cells in plates were placed in an incubator at 37°C with 5% CO_2. Cell culture medium was refreshed every 2–3 days by exchanging 100–150 µl of spent medium with fresh medium. Plates with prostate cells seeded into the ring trough were imaged 1 or 3 days after cell seeding using the Opera Phenix High Content Screening System (Perkin Elmer, Waltham, Massachusetts), equipped with proprietary Synchrony Optics consisting of a Nipkow spinning microlens disk in conjunction with pinhole disk and 2 sCMOS cameras. Fluorescent images for each of the 2 fluorescent tags (RFP and EGFP) were acquired using the 5× air objective (NA 0.16, HH14000402, PerkinElmer) in conjunction with 2 excitation lasers: 488 nm for EGFP and 561 nm for RFP. Confocal z-stacks

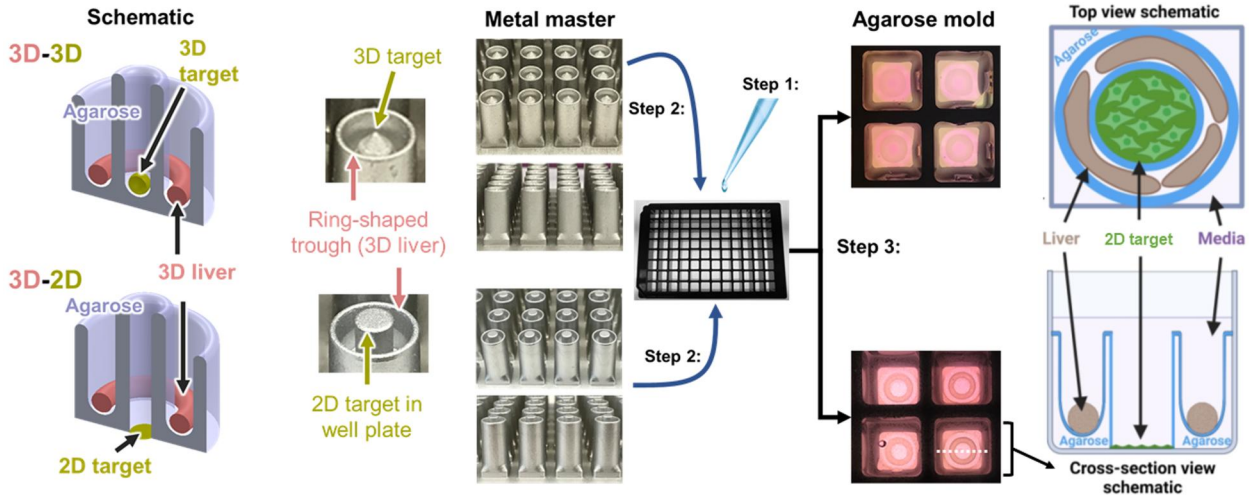

Figure 1. The design and fabrication of the 2-chamber systems (3D-3D and 3D-2D) in a 96-well plate. Left panel shows schematics of the 3D-3D and the 3D-2D 2-chamber systems made out of 2% agarose mold. Both systems consist of an outer ring-shaped trough to culture the 3D liver microtissues. The 3D-3D system has a center conical well for culturing target cells as a 3D microtissue. The 3D-2D system has a center opening to the surface of the 96-well plate, where target cells can be cultured as a 2D monolayer of cells. The middle panel shows the stainless-steel master molds that are used to create the agarose 2-chamber systems in the 96-well plates. The fabrication process entails 3 main steps: Step (1) molten sterile 2% agarose is pipetted into wells; step (2) stainless-steel metal master is inverted into well plate with molten agarose; step (3) once the molten agarose has solidified, the metal master is removed and serum-free cell culture medium is added into each of the wells. The right panels are the top and cross-sectional schematic representation of the 3D-2D 2-chamber coculture system in 1 well of a 96-well plate, showing cell culture media covering both chambers, thus allowing chemical in cell culture media to diffusing through the cell culture media, as well as through the 2% agarose hydrogel. Schematics are not to scale.

were acquired every 5 μm to capture the entire 3D microtissue in the ring-shaped trough. On day 4, medium was removed from each of the wells except for the volume in the ring trough chamber. Prostate cells alternate to the cell type already seeded into the ring trough (eg, BHPrE-RFP into wells with BHPrS-EGFP 3D microtissues in the ring trough) were seeded at cell density of 800–1000 cells/well in 10 μl in the 3D or 2D target chamber. Cells were allowed to first settle by gravity into the bottom of the 3D or 2D target chamber for 30 min, then an additional 150 μl of prostate cell medium was added slowly into each of the wells. Cell culture medium was refreshed every 2–3 days by exchanging 100–150 μl of spent medium with fresh medium. Plates were imaged 1, 3, 5, and 7 days after cell seeding using the Opera Phenix, as described earlier in this section.

Culture of AR-CALUX cells

Cells from the stably transfected human osteosarcoma (U2OS) cell line expressing the human AR (BioDetection Systems [BDS], Amsterdam, the Netherlands) were maintained in DMEM/F-12 supplemented with 10% FCS, 1% NEAAs, 10 units/ml penicillin, 10 μg/ml streptomycin, and 0.2 mg/ml G418 in an incubator (37°C, 5% CO_2, 100% humidity). The cells were routinely subcultured according to manufacturer's protocol when reaching 85%–95% confluency (ie, every 3–4 days) using trypsin-EDTA (Sonneveld *et al.*, 2005; van der Burg *et al.*, 2010).

3D liver microtissue formation

NoSpin-differentiated HepaRG cells (NHSPRG; lot: HNS1016; Lonza, Basel, Switzerland) were thawed and seeded into the ring-shaped trough of the agarose 2-chamber system at seeding densities ranging from 25 000 to 200 000 cells in 25 μl per well. Cells were allowed to first settle by gravity for 30 min, then 150 μl of Williams E medium supplemented MHTAP HepaRG supplement (Lonza), 1% GlutaMax (35050061, ThermoFisher), and 1% penicillin/streptomycin (Gibco 15140-122) was added slowly into each of the wells. Plates with seeded HepaRG cells were then placed atop an orbital rotator (36 rpm, Orbi-Shaker CO_2, Benchmark Scientific, Sayreville, New Jersey) inside an incubator at 37°C with 5% CO_2 for the duration of the entire experiment. The coculture system with HepaRG cells remained atop the orbital rotator at 36 rpm for all experiments described in this study. The plates were incubated overnight, where the seeded HepaRG cells formed 3D human liver tissues. About 100–150 μl of medium was changed with Williams E medium supplemented with 1 of the 3 HepaRG supplements (MHTAP, MHPIT, or MHMET; Lonza) on day 1 and every 24 or 48 h for 3, 6, 10 or 17 days. Throughout this manuscript, "MHTAP," "MHPIT," or "MHMET" will be used as abbreviations for HepaRG complete medium supplemented with MHTAP, MHPIT, or MHMET HepaRG supplements, respectively. Undifferentiated HepaRG cells were passaged and seeded into agarose molds in the same fashion as the NoSpin HepaRG cells and formed 3D microtissues as the undifferentiated liver control.

Cross-sectional area analysis

Brightfield images were acquired on the Opera Phenix using the 5× air objective every 30 μm. A maximum projection was built in Harmony 4.9 (Perkin Elmer) and a pipeline was created to analyze the area of the microtissues. The pipeline (Supplementary data) identified objects based on texture and then based on morphological and position properties eliminated objects that were not microtissues. Once microtissues were identified, the area was calculated.

Gene expression analysis

Plates with HepaRG microtissues were quenched on ice and remained on ice during the tissue collection process. Medium was removed, and the tissues that remained in the agarose 2-chamber system were then washed with 3 rounds of ice-cold PBS, and transferred into 1.5 ml collection tubes with a wide bore pipette tip. Tissues were then centrifuged at 600 × g at 4°C for

10 min to remove most of the PBS prior snap freezing in liquid N_2. Tissues were stored at −80°C until analysis for the gene expression of Phase I cytochrome P450 enzymes (*CYP1A1*, *CYP1A2*, *CYP2B6*, *CYP2C9*, and *CYP3A4*).

RNA was extracted from frozen tissues with MagMax mirVana total RNA isolation kit (A27828, ThermoFisher Scientific/Applied Biosystems, Bedford, Massachusetts) following the manufacturer's user guide for cells. Frozen tissues were mixed with 200 µl of lysis buffer by pipetting up and down 5 times, then transferred to KingFisher Flex 96 Deep-Well Plates (A43075, ThermoFisher). About 20 µl of binding beads were added to each lysate. The remaining steps for precipitation, washing, DNase treatment, and elution were carried out on the KingFisher flex magnetic particle processor (ThermoFisher).

Premixed TaqMan assays were purchased from ThermoFisher Scientific (4331182, Invitrogen, Carlsbad, California). Probes for gene of interest (GOI) were labeled with FAM-MGB: *CYP1A1* (Hs01054796_g1), *CYP1A2* (Hs00167927_m1), *CYP2B6* (Hs04183483_g1), *CYP2C9* (Hs04260376_m1), and *CYP3A4* (Hs00604506_m1); housekeeping gene *ACTB* (Hs01060665_g1) was used for normalization of gene expression and was labeled with VIC-MGB. The Bi-Plex reactions were set up using SuperScript III Platinum One-Step qRT-PCR kit (11732020, Invitrogen) and performed on a BioRad C1000 Touch Thermal Cycler with CFX-384 optics module (BioRad, Hercules, California). Each 10 µl reaction contains 2 µl of RNA, 5 µl of reaction mix, 0.2 µl of SuperScript III RT/Platinum Taq Mix, 0.5 µl of 20× GOI, and Actb assay mix. cDNA was synthesized for 15 min at 50°C, followed by 95°C for 2 min, then 40 cycles of 15 s at 95°C for denaturation, 30 s at 60°C for annealing and extension. Delta CT was used for calculation of relative expression for each GOI: 2 ($Actb_{CT}$-GOI_{CT}), assuming that the PCR is operating at 100% efficiency, which means the amount of product doubles perfectly during each cycle for both GOI and *Actb*.

Chemical treatments

Phenacetin (P294580; lot: 14-MWC-138-1; Toronto Research Chemicals, Toronto, Canada), bupropion hydrochloride (B689625; lot: 12-GHZ-18-1; Toronto Research Chemicals), and verapamil hydrochloride (V125000; lot: 11-XJZ-55-1; Toronto Research Chemicals) were first reconstituted in sterile DMSO (Sigma Aldrich, D2650) at concentrations of 20 to 200 mM as stock solutions. To examine chemical metabolism by HepaRG microtissues in the 2-chamber system, wells with or without HepaRG microtissues with a total volume of 250–300 µl/well were treated with one of the chemicals in HepaRG medium supplemented with MHPIT at the following final concentrations and incubation times based on prior published work (Hoekstra *et al.*, 2013; Jackson *et al.*, 2016; Ramaiahgari *et al.*, 2017; Tracy *et al.*, 1999; Turpeinen *et al.*, 2009; Yeo and Yeo, 2001): phenacetin (125 µM for 24 h or 400 µM for 3 h), bupropion (100 or 200 µM for 24 h, or 400 µM for 3 h), verapamil (20 or 30 µM for 24 h), testosterone (T1500, Sigma Aldrich; 200 µM for 2 h), or 7-ethoxycoumarin (E1379, Sigma Aldrich; 100 µM for 1 h). The final DMSO concentration from the chemical treatments was 0.2%. Reactions were quenched by placing plates directly on ice, and plates remained on ice during the entire medium and tissue collection. Medium was collected into 1.5 ml tubes, snapped frozen in liquid N_2, and stored at −80°C until analysis by LC-MS/MS. Tissues that remained in the agarose 2-chamber system were then washed with 3 rounds of ice-cold PBS, and transferred into 1.5 ml collection tubes with a wide bore pipette tip. Tissues were then centrifuged at 600 × g at 4°C for 10 min to remove most of the PBS prior to snap freezing in liquid N_2. Tissues were stored at −80°C until analysis by LC-MS/MS. We acknowledge that verapamil being both a substrate (VandenBrink and Isoherranen, 2010), and a moderate inhibitor (Chen *et al.*, 2011; Hanke *et al.*, 2020) of CYP3A4 enzyme could confound our evaluation of CYP3A4 enzyme function.

Liquid chromatography-mass spectrometry analysis to evaluate metabolites

Liquid chromatography-mass spectrometry (LC-MS/MS) analyses were completed in 2 separate sites: (1) Unilever, Sharnbrook, United Kingdom; and (2) Corteva, Inc., Indianapolis, Indiana.

Unilever

Analytical standards of phenacetin, acetaminophen, bupropion, hydroxybupropion, verapamil, norverapamil, testosterone, 6β-hydrotestosterone, 5α-dihydrotestosterone, androstenedione, acetaminophen-d_4, bupropion-d_9, hydroxubupropion-d_9, $^{13}C_3$-testosterone, 6B-hydroxytestosterone-d_3, and 5α-dihydrotestosterone-d_3, were sourced from Merck (UK). Phenacetin-d_5 was from Santa Cruz Biotechnology (USA). Verapamil-d_7 and Norverapamil-d_7 were supplied by Toronto Research Chemicals (Canada). Cell culture medium used to prepare standards and QCs for LC-MS/MS analysis consisted of 435 ml Eagle's minimum essential medium (EMEM) (Gibco, UK), 50 ml heat inactivated fetal bovine serum (Gibco, UK), 5 ml L-Glutamine (Sigma, UK), 5 ml nonessential amino acids (Gibco, UK), and 5 ml penicillin-streptomycin (10 000 U/ml in normal saline) (Sigma, UK).

To quantify substrate and metabolite concentrations in medium samples, 50 µl aliquots were mixed with 150 µl of working internal standard (deuterated analogs of each analyte, specified below) and centrifuged (3000 rpm for 5 min) prior to LC-MS/MS analysis. For tissue samples, the entire microtissue was quantitatively transferred to a homogenizer tube (Precellys CK-14-2 ml) containing ceramic beads. About 150 µl internal standard and 100 µl 75/25 (%, v/v) acetonitrile/water were added to the tube which was processed on a Precellys-24 homogenizer in 2 10 s bursts of 6400 rpm with 30 s resting in between bursts to avoid overheating of samples and equipment. Samples were cooled on ice, transferred to a suitable tube, centrifuged (3000 rpm for 10 min), and then analyzed by LC-MS/MS.

LC-MS/MS analysis, to quantify substrate and metabolite concentrations in both medium and tissues, was carried out using either a Waters Xevo TQ-S or Waters Xevo TQ-XS mass spectrometer connected to a Waters Acquity UPLC system. Chromatographic separation was achieved using a Waters Acquity BEH C18 (50 × 2.1 mm, 1.7 µm particle size) column, using a gradient from 0.1% formic acid (VWR) in water (Biosolve Chimie, Dieuze, France.) to acetonitrile with a flow rate of 0.5 ml/min and a column temperature of 40°C. The MS was operated in positive electrospray mode acquiring specific multiple reaction monitoring (MRM) mass transitions optimized using analytical standards.

Phenacetin and acetaminophen were analyzed using a gradient from 100% 0.1% formic acid in water to 100% acetonitrile between 0.2 and 1.6 min, holding at 100% acetonitrile for a further 0.2 min before returning to the starting conditions. MRM mass transitions were as follows: acetaminophen: 152 > 110; acetaminophen-d_4: 156 > 114; phenacetin: 180 > 138; and phenacetin-d_5: 186 > 143. Calibration standards were prepared in medium across the range 0.3–300 µM phenacetin and 0.01–10 µM acetaminophen. The working internal standard solution contained phenacetin-d_5 and 50 µM and acetaminophen-d_4 at 1 µM in acetonitrile.

For bupropion and hydroxybupropion, a similar LC gradient was employed as for phenacetin and acetaminophen, except that between 0.2 and 1.5 min, the composition changed to 50% 0.1% formic acid in water/50% acetonitrile before reaching 100% acetonitrile at 1.6 min and continuing as before. The MS was set to analyze MRM mass transitions as follows: bupropion: 240 > 131; bupropion-d_9: 249 > 131; hydroxybupropion 256 > 139; and hydroxybupropion-d_6: 262 > 139. The calibration ranges were 0.15–150 μM bupropion and 0.01–10 μM hydroxybupropion in media. The working internal standard solution contained bupropion-d_9 and hydroxybupropion-d_6 each at 0.5 μM in acetonitrile.

Verapamil and norverapamil utilized an identical LC gradient to that used for bupropion and hydroxybupropion. MRM mass transitions were verapamil: 455 > 165; verapamil-d_7: 462 > 165; norverapamil: 441 > 165; and verapamil-d_7: 448 > 165. Calibration ranges were 0.075–19.5 μM verapamil and 0.006–1.56 μM for norverapamil with a working internal standard solution prepared in acetonitrile which contained verapamil-d_7 and norverapamil-d_7, each at 0.005 mM.

For testosterone and metabolites, the LC gradient was held at 10% 0.1% formic acid in water/90% acetonitrile for 0.3 min before ramping to 100% acetonitrile at 1.5 min and holding for 0.3 min, after which time the composition was returned to the starting conditions. MRM transitions in positive electrospray ionization (ESI) were as follows: Testosterone: 289 > 97; 6β-hydroxytestosterone: 305 > 269; 5α-dihydrotestosterone: 291 > 255; androstenedione: 287 > 97; $^{13}C_3$-testosterone: 292 > 100; 6β-hydroxytestosterone-d_3: 308 > 272; and 5α-dihydrotestosterone-d_3: 294 > 258. Additionally, although no analytical standard could be sourced, a speculative MRM was included for testosterone glucuronide: 465 > 279. Calibration ranges were from 0.25 nM (testosterone and androstenedione) or 1.25 nM (6β-hydroxytestosterone and 5α-dihydrotestosterone) to 50 nM (all analytes). A working internal standard solution was prepared in acetonitrile containing $^{13}C_3$-testosterone, 6β-hydroxytestosterone-d_3, and 5α-dihydrotestosterone-d_3 each at 1 nM.

All calibration standards were analyzed at the beginning and end of each analytical run and used to construct a calibration graph of concentration versus peak area ratio (analyte/internal standard) for each analyte. The concentrations in samples, standards, QC samples (media fortified with analytes at 3 concentrations analyzed in duplicate) and blanks (media only) were calculated from the calibration graph. For tissue samples, because calibration standards were prepared in medium, the concentration measured by LC-MS/MS was in μM (nmols/ml) based on a 50-μl aliquot. This was converted to nmols per tissue sample by dividing by 20.

Based on FDA (FDA, 2018) and ICH (ICH, 2022) guidelines, standards with a measured concentration that deviated from nominal by >20% were excluded from the calibration with a maximum of 25% of standards rejected in order for results to be accepted. Method performance was verified by the analysis of independently prepared quality control samples prepared in medium at 3 concentrations and analyzed in duplicate, quantified against the calibration, with the measured concentration in at least 4 out of 6 (including at least 1 at each concentration) being within 20% of nominal. Blank media analyzed with the samples contained no significant interferences.

Corteva

Sample preparation was done using simple dilution 20 μl of sample that was diluted into 180 μl of 70/30 acetonitrile (A955, Fisher Scientific)/water (W64, Fisher Scientific). A calibration curve was prepared in matrix and diluted to match the sample preparation. The limit of quantification for each compound was as follows: testosterone (standard: T-037, Cerilliant, Round Rock, Texas) 1 ng/ml, 6β-hydroxytestosterone (standard: H-059, Cerilliant) 10 ng/ml, 7-EC (standard: E1379, Sigma Aldrich) 100 ng/ml, 7-HC (standard: H24003, Sigma Aldrich) 5 ng/ml, 7-HC glucuronide (standard: SC-210617, ChemCruz, Dallas, Texas) 1 ng/ml, acetaminophen (standard: 1003009, Sigma Aldrich) 5 ng/ml, and phenacetin (standard: 77440, Sigma Aldrich) 5 ng/ml.

An Agilent 1290 Infinity II ultra-high-performance liquid chromatography (UHPLC) instrument was connected to an Agilent 6495A mass spectrometer for LC-MS/MS analysis. The UHPLC system consisted of Agilent 1290 Infinity II binary pump, Agilent dual needle multisampler, and Agilent column compartment. The column used was a Phenomenex Luna Omega 3 μm Polar C18 100°A, 3 × 100 mm, 3 μm particle size (00D-4760-Y0, Phenomenex). Acetonitrile with 0.1% formic acid (LS120, Fisher Scientific) and water with 0.1% formic acid (LS118, Fisher Scientific) and 0.25 mM ammonium fluoride (2160211, Sigma Aldrich) were the mobile phases used. The flow rate was set to 700 μl/min, the autosampler was set to 10°C, and the injection volume used was 5 μl. The sample analysis used a gradient separation starting at 20% B and increased to 40% over 10 min and then to 75% over 2 min and then to 95% over 0.1 min. The gradient was then held at 95% B for 2 min returned to 20% over 0.1 min and held for 2 min to equilibrate the column for the next injection.

The mass spectrometer parameters were optimized for this analysis using ESI. Nitrogen drying gas was set at 16 l/min and 250°C. The sheath gas temperature was set to 275°C with a flow of 12 l/min. The nebulizer flow rate was optimized to be 60 psi, and the ion funnel parameters were 100 HRF 80 LRF in both positive and negative modes. The capillary voltage was set to 5500 V in positive mode and 3000 V in negative mode. Nozzle voltage in positive mode was 2000 and 500 V in negative mode. The collision energies (CE) were optimized for each MRM. All analytes analyzed in positive mode. The MRMs and CEs used for each analyte were: testosterone 289.2–108.9 CE24, 6β-hydroxytestosterone 305.2–269.1 CE12, 7-EC 191.1–163.0 CE28, 7-HC 163.0–107.1 CE35, 7-HC Gluc 339.0–163.0 CE12, acetaminophen 152.1–110.0 CE14, and phenacetin 180.1–110.0 CE 20.

All standards were analyzed at the beginning of the analytical run after a blank matrix sample. A calibration curve was constructed from the analysis of these standards using concentration versus peak area. A minimum of 5 calibration points were used for the construction of the calibration curve. The concentrations of the standards, samples, and QC samples were calculated from the calibration curve.

Standards that deviated by more than 20% were excluded from the calibration curve, based on FDA (FDA, 2018) and ICH (ICH, 2022) guidelines. To ensure method performance, a minimum of 2 QC levels prepared independently of the standards in triplicate were used. The acceptance criteria for the QC samples that they must be within 20% of the nominal value. At least 1 QC for each level must be within 20% of nominal and a minimum of 75% of the QCs must pass to ensure the calibration was accurate. QCs were analyzed throughout the run to ensure the method performance was consistent. Blank matrix and blank diluent samples were analyzed throughout the run to ensure there were no interferants or carryover present.

Histology and immunohistochemical analyses

Medium was removed from each well, then 200 μl of 10% neutral buffered formalin (427098, ThermoFisher) was added to each

well to fix the HepaRG microtissues for 30 min, followed by 3 10-min incubations with 200 µl of 1× PBS. The PBS was then removed and replaced with 200 µl of 70% ethanol per well then stored at 4°C. The gels were capped with molten but cooled 2% agarose, embedded in paraffin, sectioned (5 µm), stained with hematoxylin and eosin (H&E) for general morphology. H&E-stained slides were scanned with the Aperio digital pathology slide scanner (Leica Biosystems Inc, Buffalo Grove, Illinois) or with the Olympus VS200 Slide Scanner (Olympus Life Science, Waltham, Massachusetts) for morphological analysis.

Slides were also immunostained for albumin (ab2406, Abcam, Cambridge, Massachusetts), asialoglycoprotein receptor (ASGR2) (no. 13908, SinoBiological, Wayne, Pennsylvania) for glycoprotein uptake, Phase I cytochrome P450 (CYP3A4) (ab124921, Abcam) enzyme, and multidrug resistance-associated protein 2 (MRP2) (Abcam, ab187644) transporter for biliary excretion on a Ventana Discovery Ultra automated IHC/ISH research slide staining system (Roche Diagnostics, Indianapolis, Indiana) and counterstained with hematoxylin (no. 760-2021, Roche Diagnostics, Indianapolis, Indiana). A set of slides were stained using the Periodic acid-Schiff (PAS) (no. 9162B, Newcomer Supply, Middleton, Wisconsin) stain with or without diastase (alpha-amylase) enzyme (no. 1905B, Newcomer Supply). H&E-stained slides were scanned with an Aperio digital pathology slide scanner (Leica Biosystems Inc, Buffalo Grove, Illinois) or with an Olympus VS200 Slide Scanner (Olympus Life Science, Waltham, Massachusetts) for morphological analyses. Immunostained and PAS-stained slides were mounted with Polymount-Xylene (Polysciences, Inc., Warrington, Pennsylvania) and a glass cover slip. Mounted slides were imaged on a Leica DM5000B upright microscope equipped with a Leica DFC 7000T camera (Leica Microsystems) using LAS X software (version 3.7.4.23463).

Transmission electron microscopy

Microtissues were fixed in 1 ml 3% glutaraldehyde (no. 18436, Ted Pella, Redding, California) in 100 mM cacodylate buffer (no. 11652, Electron Microscopy Sciences) at room temperature (RT) for 1 h, then stored at 4°C. Microtissues were washed in cacodylate buffer and post-fixed in 1% osmium textroxide solution (no. 18463, Ted Pella), 0.3 g potassium ferricyanide (no. P232-500, Fisher Scientific) in deionized water. Samples received microwave treatment (150 W × 1 min, 0 W × 1 min-10 cycles) using a Pelco BioWave and then were placed on a rocker for 35 min at RT. Samples were rinsed in MilliQ water, then 1% uranyl acetate solution (no. 22400, Electron Microscopy Sciences) was added to each vial (1 ml), and samples were placed on a rocker for 1 h in the dark. Samples were rinsed in MilliQ water and stored at RT overnight. Samples were dehydrated with a graded ethanol series at RT with continuous slow rotation at 4°C, and then infiltrated in a graded series of LR white resin (Polysciences, no. 17411-500) in ethanol at 4°C with continuous slow rotation. Individual microtissues were moved to flat-bottomed polyethylene capsules (TAAB, EMS) and polymerized at 50°C for 3 h. These flat-bottomed blocks were trimmed to a pyramidal shape with a Leica EM TRIM2, and then faced with a dry diamond knife on a Leica UC7 ultramicrotome. Thin sections (500 nm thick) made with a diamond knife on a Leica UC7 ultramicrotome and were collected onto poly-L lysine coated ITO slides (no. CG-811N-S115, Delta Technologies, Loveland, Colorado). Slides were observed and imaged with a ThermoFisher Apreo S scanning electron microscope.

Human albumin and fibrinogen production

To evaluate human albumin and fibrinogen production by HepaRG microtissues, medium was collected into 1.5 ml protein LoBind Protein tubes (0030108442, Eppendorf, Hamburg, Germany) at selected time points, snapped frozen in liquid N_2 and stored at −80°C until analysis. Human albumin production was evaluated using a human albumin ELISA Quantitation Kit (E80-129; Bethyl, Montgomery, Texas) according to the manufacturer's protocol. Human fibrinogen production was evaluated using a human fibrinogen ELISA kit (ab241383; Abcam, Cambridge, United Kingdom) according to the manufacturer's protocol. Medium samples were first diluted 50–125 folds with assay reagent prior analysis. Human albumin production per well was represented in ng/day, or in pg per day per cell based on the number of cells seeded initially. Human fibrinogen production per well was represented in pg per day.

Agarose adsorption

To investigate the potential adsorption of albumin by the agarose component in our 2-chamber coculture system, human albumin (ab205808; lot: GR3392999; Abcam, Waltham, Massachusetts) spiked MHPIT medium was added to wells with or without agarose to achieve a final concentration of 1.8, 3.5, or 6.5 ng/ml, which are within the range of albumin production by our HepaRG microtissues that have been matured in MHPIT for 10 days. Plates were placed in an incubator at 37°C with 5% CO_2 for 24 h, then medium was collected into 1.5 ml tubes, snapped frozen using liquid N_2 and stored at −80°C until analysis by ELISA.

To investigate the potential adsorption of phenacetin by the agarose in our 2-chamber coculture system, phenacetin (P294580; lot: 14-MWC-138-1; Toronto Research Chemicals, Toronto, Canada) spiked MHPIT medium was added to wells with or without agarose to achieve a final concentration of 125 µM. Plates were placed in an incubator at 37°C with 5% CO_2 for 24 h, then medium was collected into 1.5 ml tubes, snapped frozen using liquid N_2 and stored at −80°C until analysis by LC-MS/MS.

Chemical diffusion

To examine phenacetin and acetaminophen diffusion in the 2-chamber coculture system, HepaRG microtissues after 10 days of maturation in MHPIT were incubated in phenacetin (final concentration = 125 µM) for 1, 4, or 24 h. The distance between the center of the toroid well to the bottom of the center target well is less than 3 mm. The incubation times were selected to gain a comprehensive understanding of solute distribution over time in our system, and the theoretical times for glucose to diffuse in solution (approximately 1.3 h over 3 mm) versus 2% agarose (approximately 1.8 h over 3 mm) (Lundberg and Kuchel, 1997). Reactions were quenched by placing the plates directly on ice. Plates remained on ice during the entire medium collection using 2 different methods: (1) only the top layer of medium (approximately 75 µl) per well was collected and transferred into a 1.5 ml tube; or (2) all medium including the HepaRG microtissues per well (approximately 165 µl) were collected and transferred into a 1.5-ml tube. The tubes were centrifuged at 600 × g at 4°C for 10 min, then medium was transferred to a new 1.5 ml tube. Tubes with medium were then snapped frozen using liquid N_2 and stored at −80°C until analysis by LC-MS/MS.

Two-chamber coculture system with human liver and AR-CALUX cells

We investigated the effects of human liver metabolism on testosterone-mediated activation of the androgen receptor (AR) by coculturing HepaRG cells as 3D microtissues in the ring-shaped trough, and the AR-CALUX reporter cells in the 2D target chamber, in our 2-chamber coculture platform. NoSpin-differentiated HepaRG cells were thawed and seeded into the ring-shaped trough of the agarose 2-chamber system at 50 000 cells in 25 µl per well, or with just 25 µl media as the no liver metabolism control, and cultured as described above with constant rotation (36 rpm). About 100–150 µl of medium was changed with Williams E medium supplemented with MHPIT on day 1 and every 48 h for 10 days. About 10 days post-seeding of HepaRG cells, 140 µl medium was removed from each of the wells, with the remaining media in the central chambers removed by aspiration. About 16 000 U2OS AR-CALUX cells were then seeded into the central chamber of the agarose 2-chamber system in a volume of 15 µl MHPIT media. After 10 min of allowing the AR-CALUX cells to settle to the bottom of the well onto the 2D surface, 140 µl of MHPIT media was added into each of the wells, covering both compartments within a well. Plates were returned into the incubator and cultured with constant rotation (at 36 rpm) overnight. One day after the seeding of AR-CALUX cells, 100 µl of media per well were replaced 100 µl MHPIT media spiked with either 10, 30, 100, and 1000 nM testosterone (T), or the no T vehicle control. The 2-chamber coculture system was incubated in the presence or absence of T for 24 h with constant rotation (36 rpm). After this 24-h incubation, the medium was collected from each of the wells for LC-MS/MS analysis by Unilever. The agarose hydrogels with or without the HepaRG 3D tissues were removed using a pipette tip, leaving only the AR-CALUX cells on the bottom of the each of the wells. The cells were washed with 150 µl of 1:1 PBS: millipore water solution and lysed with 30 µl lysis mix per well (cat. no.: 26; BDS, Amsterdam, The Netherlands). The plates were placed on a plate shaker at 300 rpm for 30 min, then transferred to into the Synergy H1 Hybrid Multimode (H1MM) Microplate Reader (BioTek Instruments, Inc., Vermont), where 100 µl of the Illuminate mix (cat. no.: 35; BDS) was automatically added to each well and luminescence was measured. Five independent studies were executed with 6 technical replicates per group.

Statistical analysis

SAS 9.4 software was used for statistical analyses. Data are presented as mean ± SD. $N = 3$–15 per group for all experiments. All data were first examined for equal variance and for normality using the Shapiro-Wilk test. Student's 2-sided *t* test or 1-way ANOVA with *post hoc* Tukey HSD Test, or their nonparametric equivalents, were used to evaluate the effects of different maturation times and medium supplements on HepaRG 3D microtissues gene expression and functions, as well as the differential AR-CALUX activation and testosterone metabolism in the presence or absence of HepaRG 3D microtissues. Statistical significance was set at $p \leq .05$.

Results

Design and fabrication of the 2-chamber systems (3D-3D and 3D-2D) in a 96-well plate format

A 2-chamber coculture system in a higher throughput 96-well format was designed and fabricated for the determination of toxicity on target tissues in the presence of physiologically relevant human liver metabolism (Figure 1). The hydrogel system within a single well consisted of an outer ring-shaped trough to culture human liver cells as 3D microtissues, and a central well to house target cells in 2D or 3D.

Two-chamber coculture system was effective in culturing 2 different cell types for live-cell confocal imaging with minimal cross-over between chambers

We utilized 2 types of fluorescently tagged prostate cells (epithelial cells genetically labeled with RFP; stromal cells genetically labeled with EGFP) to demonstrate the efficacy of our 2-chamber coculture system in successfully culturing cells in 2D or 3D in their respective chambers with minimal cross-over of cell types over time (Figure 2A), and to illustrate that the 3D microtissues can be effectively visualized in 3 dimensions using confocal microscopy. Figures 2B and 2C illustrate that both cell types successfully formed 3D tissues in the 3D-3D 2-chamber coculture system that are stable over time, and with minimal cross-over of cell types. Figure 2C also shows that the size of the 3D target microtissue changed with cell seeding density, suggesting the system's ability to modulate target size by simply adjusting the number of cells seeded. When cells were concurrently cultured as 3D microtissues in the ring-shaped trough and as a 2D monolayer (3D-2D coculture system), the cells remained viable over time. There was little migration of prostate epithelial cells (Figure 2D of 2 representative wells, 2F—top panels) compared with prostate stromal cells (Figure 2E of 2 representative wells, 2F—bottom panels) cultured in the 2D target chamber, reflecting the proliferative and migratory mesenchymal nature of prostate stromal cells as compared with epithelial cells (Franco *et al.*, 2011). Two-dimensional prostate epithelial cells exhibit more consistent cell morphology (D—left vs right panels, F—top-left vs top-right panels) than the 2D prostate stromal cells are highly variable in size and shape (E—left vs right panels, F—bottom-left vs bottom-right panels). The microtissues were readily imaged by confocal microscopy using 5 µm z-stacks to render reconstructed microtissues in 3D (Figure 2G).

Optimization of seeding density and cell-to-medium ratio

To engineer a 2-chamber liver-organ coculture model for the determination of toxicity on target tissues in the presence of human liver metabolism, the liver compartment of this coculture system needs to generate human-relevant metabolites in physiologically relevant concentrations, and that the target tissues/cells can be exposed to the metabolites in these relevant concentrations. The current "gold standard" for evaluating human liver metabolism *in vitro* is to expose chemicals to PHHs in suspension, in a cell density of 0.2–1 hepatocyte per nl of medium (Jackson *et al.*, 2016; Smith *et al.*, 2012).

We examined seeding densities from 25 000 to 200 000 cells/well to cover a range of cell-to-media ratios from approximately 0.1 to 0.8 cells/nl of medium. Using live-cell brightfield imaging (Figure 3A), morphological analysis with H&E staining (Supplementary Figure 1), and evaluating albumin production using ELISA (Figure 3B). Increasing cell number decreased albumin secretion on a per cell basis, thus we concluded that seeding densities greater than 100 000 cells/well were too high to maintain optimal viability and liver function. At seeding densities of 100 000 cells/well or greater, there was a significant decline in albumin production per cell, and increased cell death seen in H&E-stained sections. We evaluated the expression of liver biomarkers (albumin, ASGR2, CYP3A4, MRP2, and glycogen) by

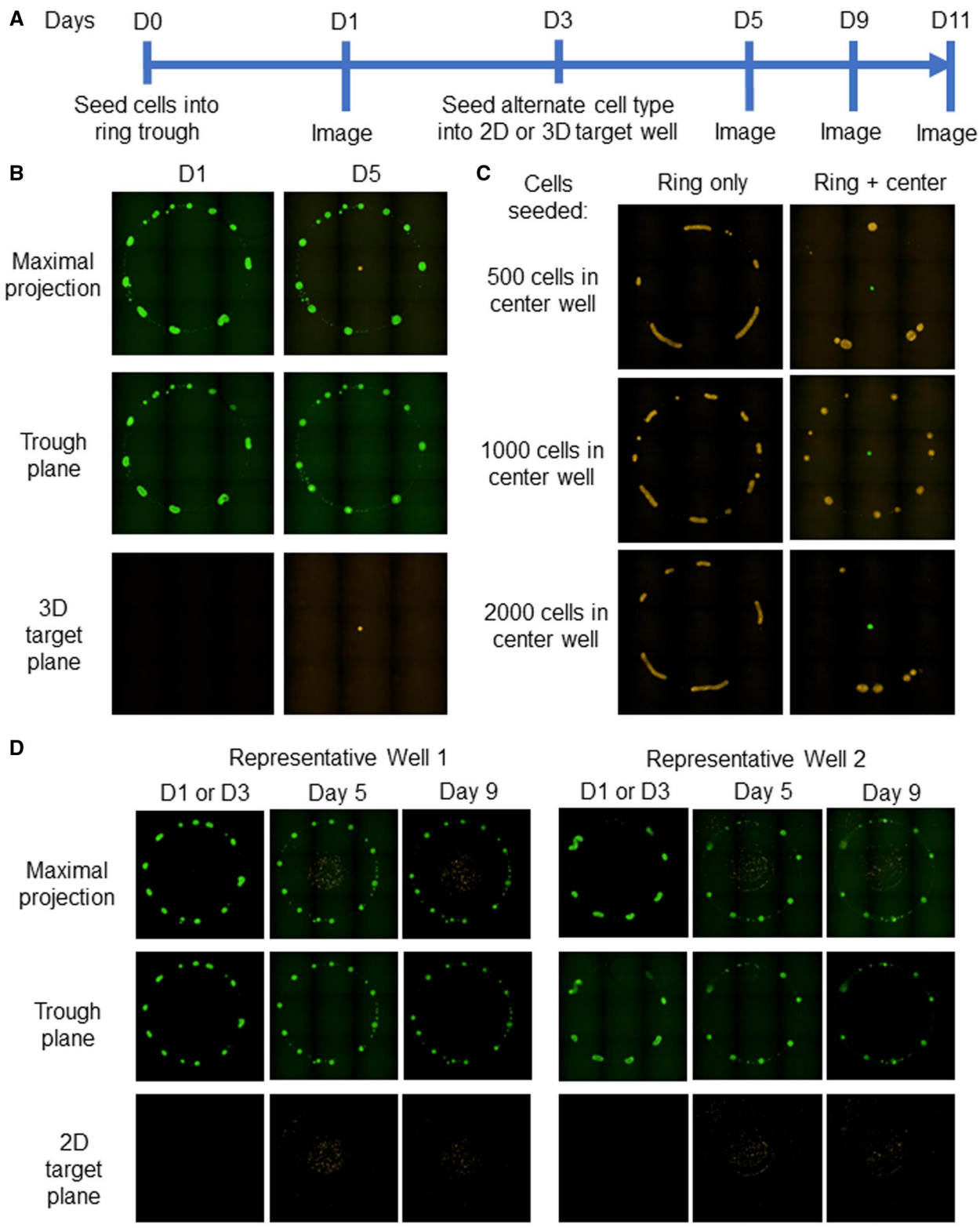

Figure 2. The 2-chamber systems allow the culture of 2 different cell types isolated within their separate compartments. Experimental timeline for examining coculture capability of the 2-chamber system (A). Prostate stromal (RFP; yellow) and epithelial (EGFP; green) cells form 3D tissues that are stable over time with minimal cross-over of cell types (B, C). The size of the 3D spheroid target microtissue can be modulated by changing the number of cells seeded (C). Prostate stromal and epithelial cells successfully form both 3D tissues and 2D monolayers of cells with minimal cross-over of cell types (D, E; 2 representative wells). Two-dimensional prostate epithelial cells exhibit consistent cell morphology (D—left vs right panels, F—top-left vs top-right panels), whereas 2D prostate stromal cells are highly variable in size and shape (E—left vs right panels, F—bottom-left vs bottom-right panels). Three-dimensional tissues are readily imaged by confocal microscopy in the x, y, and z planes (G).

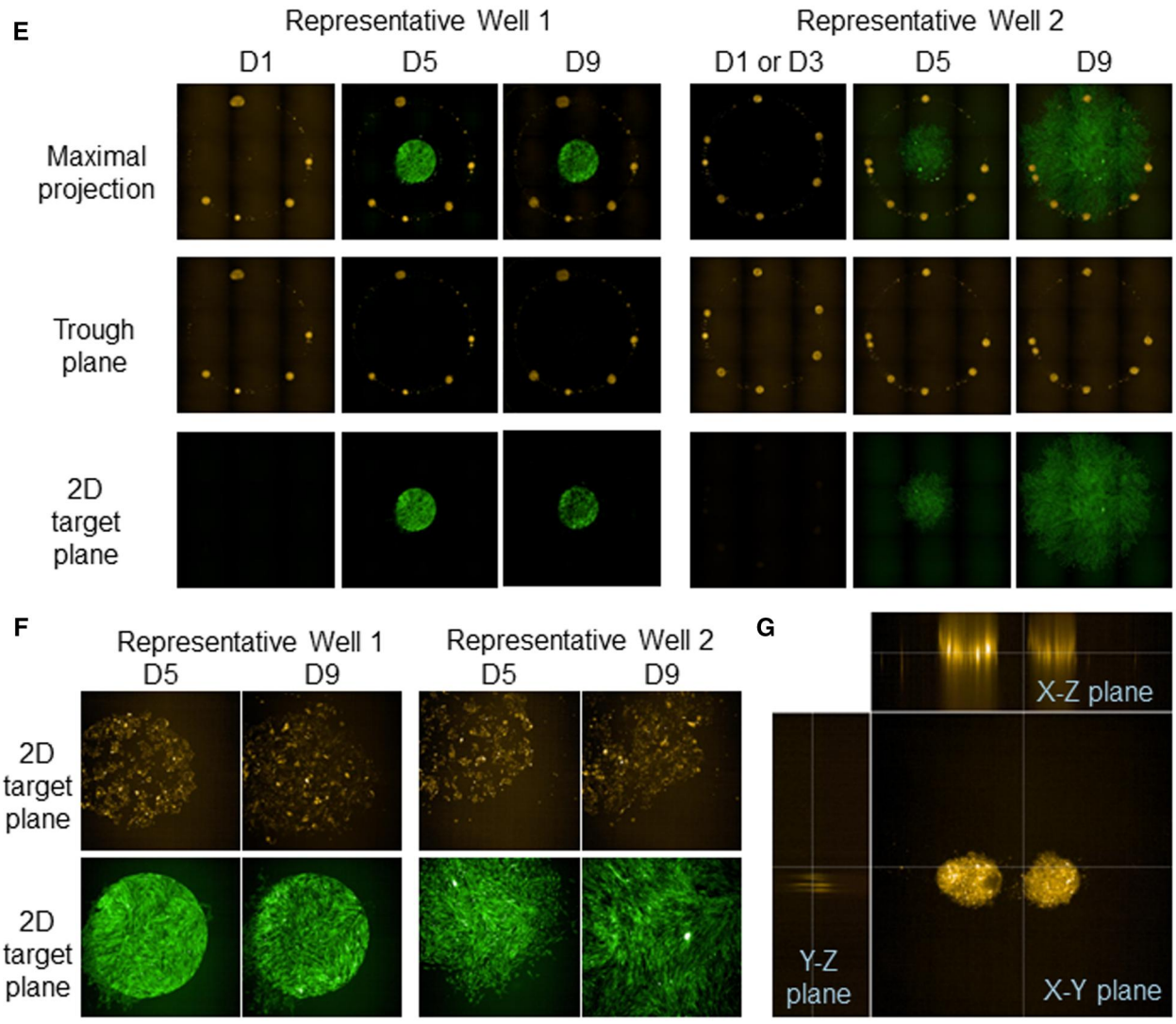

Figure 2. Continued.

immunohistochemistry (Supplementary Figure 2), gene expression (Figure 3C) of 5 hepatic Phase I enzymes (CYP1A1, CYP1A2, CYP2B6, CYP2C9, and CYP3A4), and metabolic functions of Phase I/II enzymes (Figure 3D; CYP1A2: phenacetin → acetaminophen; CYP3A4: testosterone → 6β-OH-testosterone; CYP1A2 and Phase II uridine diphosphate-glucuronosyl transferase [UGT]: 7-ethoxycoumarin → 7-hydroxycoumarin glucuronide). The measurement of medium levels of 7-hydroxycoumarin glucuronide (7-HCG) in 7-ethoxycoumarin (7-EC)-treated HepaRG microtissues was used to evaluate the combined function of CYP1A2 and UGT enzymes, where tissues exposed to 7-ethoxycoumarin (7-EC) is first metabolized to 7-hydroxycoumarin (7-HC) by CYP1A2 (not measured), and 7-HC is subsequently metabolized to 7-hydroxycoumarin glucuronide (7-HCG) by UGT (Sudo *et al.*, 2017). These results indicated that 50 000 cells/well was an optimal seeding density for this coculture system, a cell-to-medium ratio of approximately 0.2 cells/nl. Figure 3E shows live-cell brightfield images and the cross-sectional area measurements of microtissues (arrows) formed with 50 000 HepaRG cells, which remained stable and compacted over the course of 17 days. Prior work showed that culturing HepaRG cells in 3D required a minimum of 10 days in culture for recovery/differentiation to reach a steady state in metabolic functions (Jackson *et al.*, 2016; Ramaiahgari *et al.*, 2017). Microtissues of 10-day old HepaRG microtissues at 50 000 cells/well were characterized using various liver-relevant biomarkers (Figure 3F) and transmission electron microscopy (Figure 3G).

HepaRG 3D microtissue Phase I CYP gene expression, and Phase I/II enzyme function

We executed a time-course experiment to elucidate how hepatic Phase I CYP gene expression and metabolic function of HepaRG microtissues in the 2-chamber system were modulated over 17 days of maturation when cultured in MHPIT. HepaRG cells were cultured in the ring compartment for 3, 6, 10, or 17 days prior to tissue collection for RNA extraction (Figure 4A), or to tissue exposure to model compound to evaluate function of CYP1A2 (Figure 4B), CYP2B6 (Figure 4C), CYP3A4 (Figure 4D), and the combination of CYP1A2 and UGT enzymes (Figure 4B). The relative gene expression of *Cyp* enzymes in day 10 HepaRG microtissues followed a similar pattern as the relative abundance of CYP enzymes in human hepatic tissues (Pelkonen *et al.*, 2008): *Cyp3A4* ≫ *Cyp2c9* > *Cyp1a2* >= *Cyp2b6*. Maturation time modulated the gene expression of Phase I enzymes; *Cyp1a1* and *Cyp1a2*

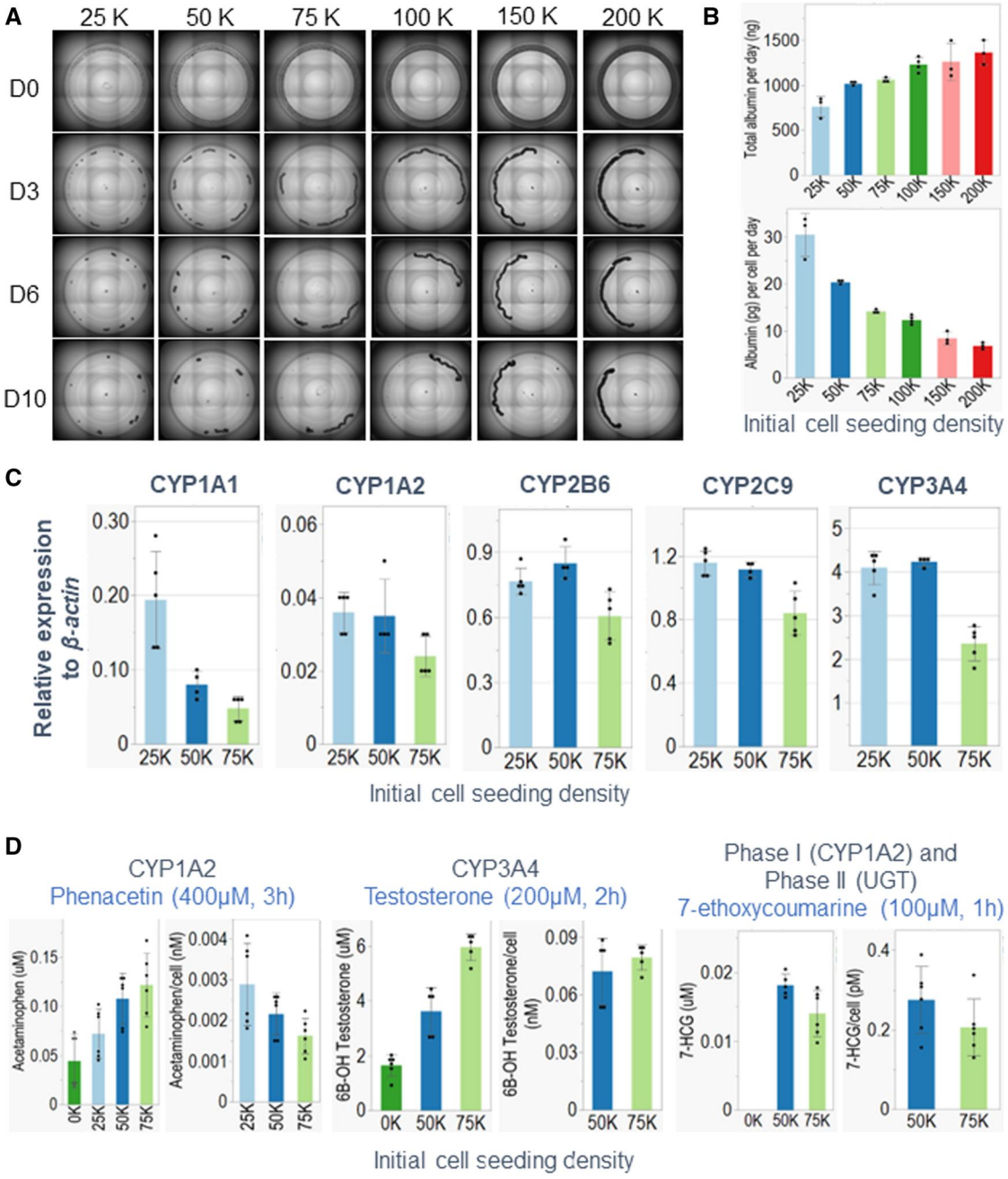

Figure 3. Optimization of HepaRG seeding densities in 2-chamber systems. Seeding densities of HepaRGs from 25 000 to 200 000 cells per well were examined in the 2-chamber systems. A, Representative live cell brightfield images showing HepaRG cells forming 3D microtissues during culture in the 2-chamber system for 0, 3, 6, and 10 days. B, Graphical representation of total albumin secreted per day (ng) and the corrected secreted albumin per number of cells initially seeded (pg/d) after 10 days of maturation, showing that increasing cell seeding density decreased albumin secretion on a per cell basis. C, Decline in hepatic Phase I CYP enzyme gene expression of HepaRG 3D microtissues matured for 10 days when the initial seeding density increased from 50 000 to 75 000 cells per well. D, Decline in hepatic Phase I/II enzyme function of HepaRG 3D microtissues matured for 3 days (phenacetin) or 10 days (testosterone; 7-ethoxycoumarin) when the initial seeding density increased from 25 000 or 50 000 to 75 000 cells per well. E, Representative brightfield images of HepaRG 3D microtissues at an optimal seeding density of 50 000 cells per well-formed stable 3D microtissues (arrows) that compacted over the course of 17 days, as indicated by the decline in cross-sectional area of the brightfield imaged tissues. F, HepaRG microtissues (day 10) were formalin-fixed, paraffin-embedded and sectioned for histological analyses. Hematoxylin and eosin (H&E) staining shows HepaRG cells in 3D microtissues have abundant cytoplasm. Immunohistochemical staining (in brown) reveals tissue expression of albumin, asialoglycoprotein receptor (ASGR2) for glycoprotein uptake, Phase I cytochrome P450 (CYP3A4) enzyme, and multidrug resistance-associated protein 2 (MRP2) transporter for biliary excretion. Periodic acid-Schiff (PAS) stain with or without diastase enzyme that breaks down glycogen supports that HepaRG microtissues synthesize and store glycogen. G, Transmission electron microscopy (scale bar = 2 μm) showing characteristic features of mature hepatocytes; the inset is a higher magnification the tight junctional apparatus associated with the bile canaliculus. BC, bile canaliculus; M, mitochondria; Mv, microvilli; N, nucleus; PM, plasma membrane; TJ, tight junction; UGT, Phase II uridine diphosphate-glucuronosyl transferase; 7-HCG, 7-hydroxycoumarin glucuronide.

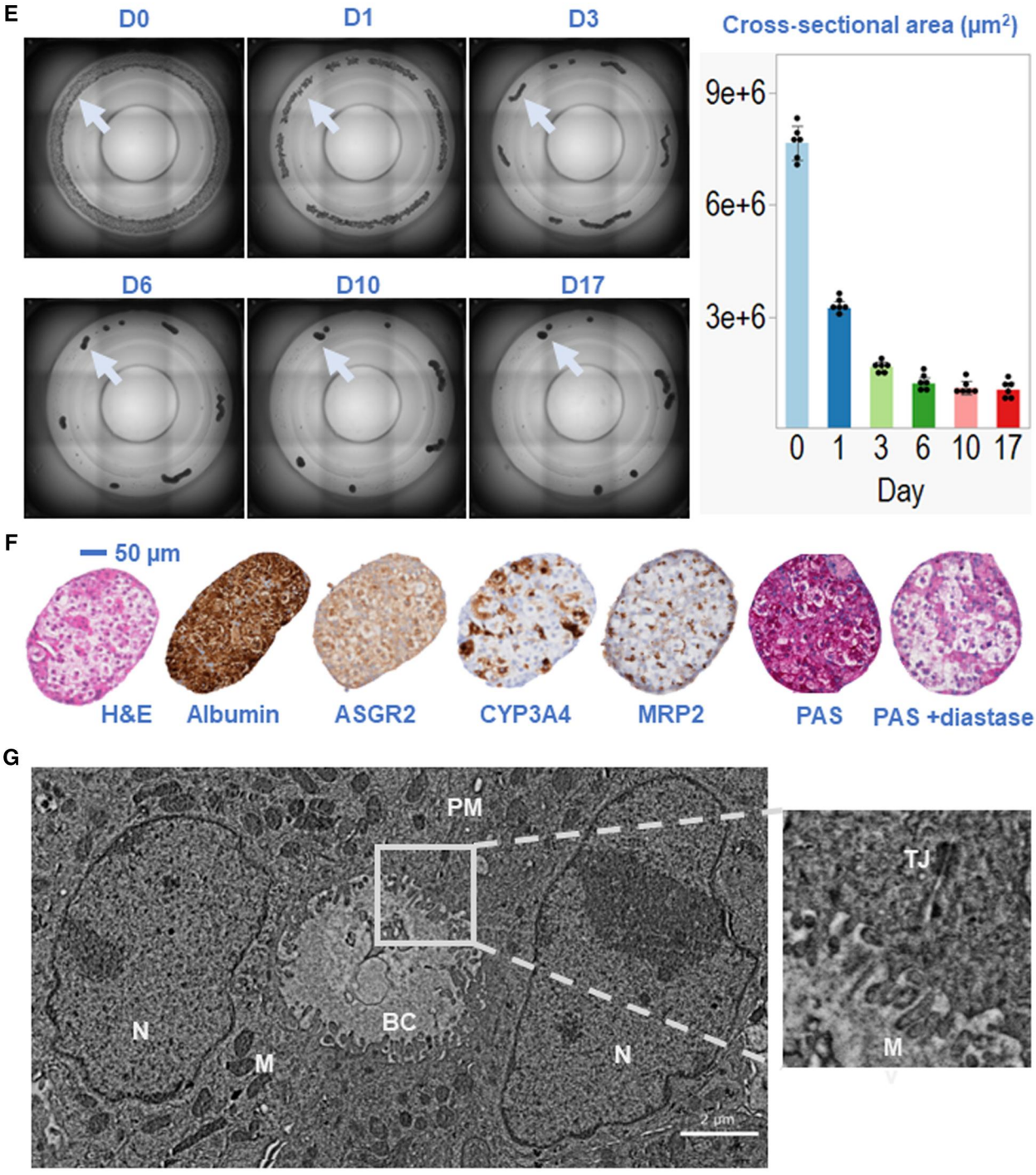

Figure 3. Continued.

gene expression peaked on day 3, then declined over time. *Cyp2b6* gene expression peaked on day 6, and *Cyp2c9* and *Cyp3a4* gene expression increased incrementally over the course of 17 days. However, CYP enzyme function did not necessarily correspond with gene expression.

Zonation-like characteristics of HepaRG microtissues can be modulated by medium conditions

Mature mammalian liver exhibits zonation to maintain optimal metabolic homeostasis, with general metabolic functions enhanced in the periportal zone and greater metabolism of drugs and xenobiotics in the perivenous zone (Lindros, 1997; Oinonen and Lindros, 1998; Torre *et al.*, 2010). This study demonstrated that HepaRG microtissues in the 2-chamber system recapitulates an *in vivo*-like zonation xenobiotic metabolism simply by maturing in different medium supplements that have varying amounts of DMSO (MHTAP, 0%; MHPIT, 0.5%; MHMET, 1.67%). HepaRG microtissues in the 2-chamber system demonstrated increasing Phase I xenobiotic gene expression (Figure 5A) and enzyme function (Figure 5B), as well as CYP3A4 protein expression (Figure 5C),

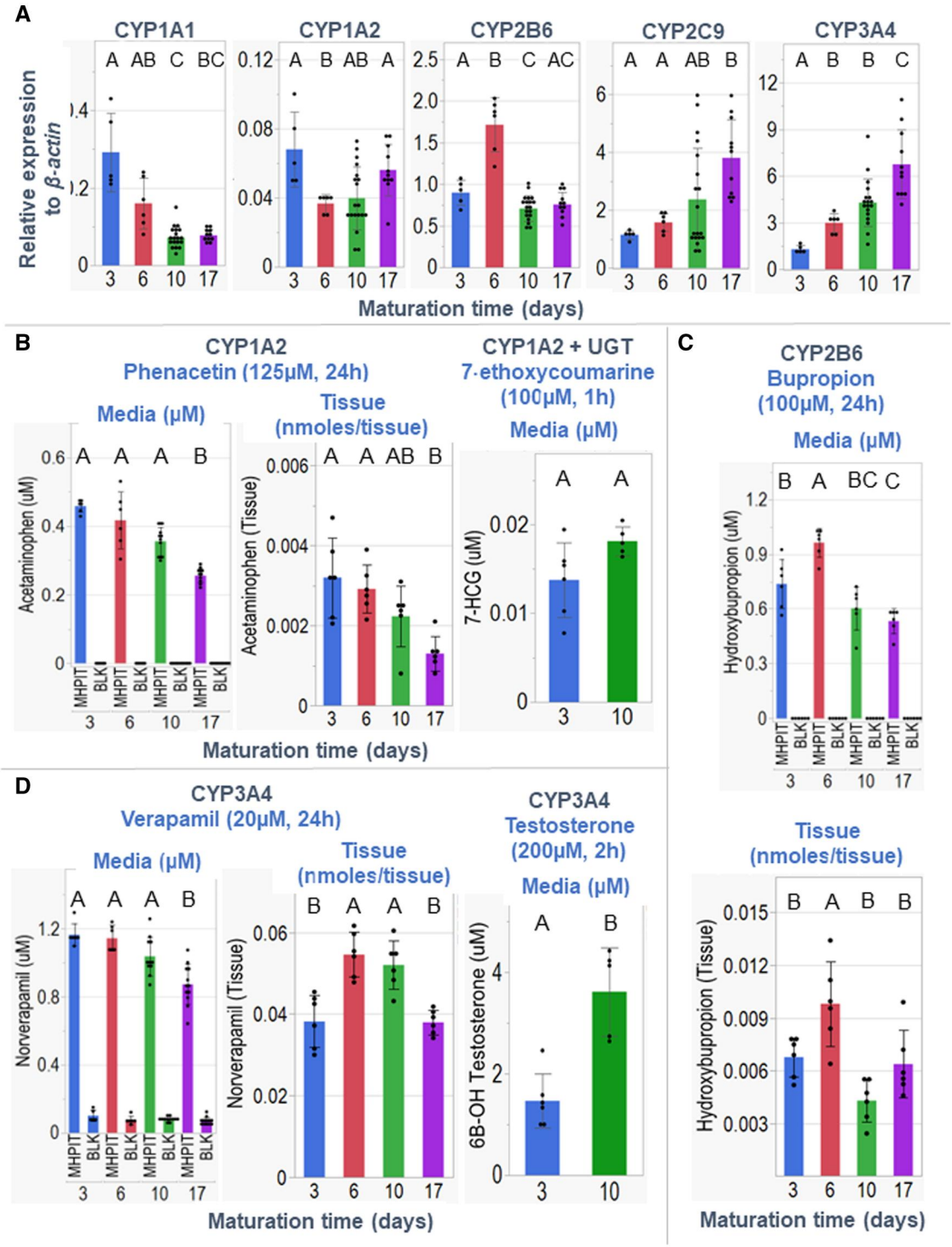

Figure 4. HepaRG 3D microtissue gene expression and function are dependent on the time of HepaRG maturation. Gene expression relative to housekeeping gene β-actin (A). Metabolic function (B–D) of hepatic Phase I/II enzymes in HepaRG 3D microtissues that have matured in the ring trough for 3, 6, 10, or 17 days. CYP1A2, CYP2B6, CYP3A4, and the combined CYP1A2 + UGT functions were evaluated by incubating HepaRG 3D microtissues with phenacetin (125 μM for 24 h), bupropion (100 μM for 24 h), verapamil (20 μM for 24 h), testosterone (200 μM for 2 h), or 7-ethoxycoumarin (100 μM for 1 h), respectively. Data = mean ± SD. Student's *t* test and 1-way ANOVA with *post hoc* Tukey HSD test, or their nonparametric equivalent, were used to examine statistical significance between maturation days. Bars that do not share the same letters are significantly different (p value $\leq .05$). 7-HCG, 7-hydroxycoumarin glucuronide; UGT, Phase II uridine diphosphate-glucuronosyl transferase.

with increasing DMSO. The opposite pattern is true for the expression of proteins involved in general metabolism, where increasing DMSO decreased total albumin (Figure 5D) and fibrinogen (Figure 5E) production.

Agarose did not alter medium constituent concentration or chemical diffusion

For the liver 3D microtissues in the 2-chamber system to effectively metabolize chemicals and expose target cells, free

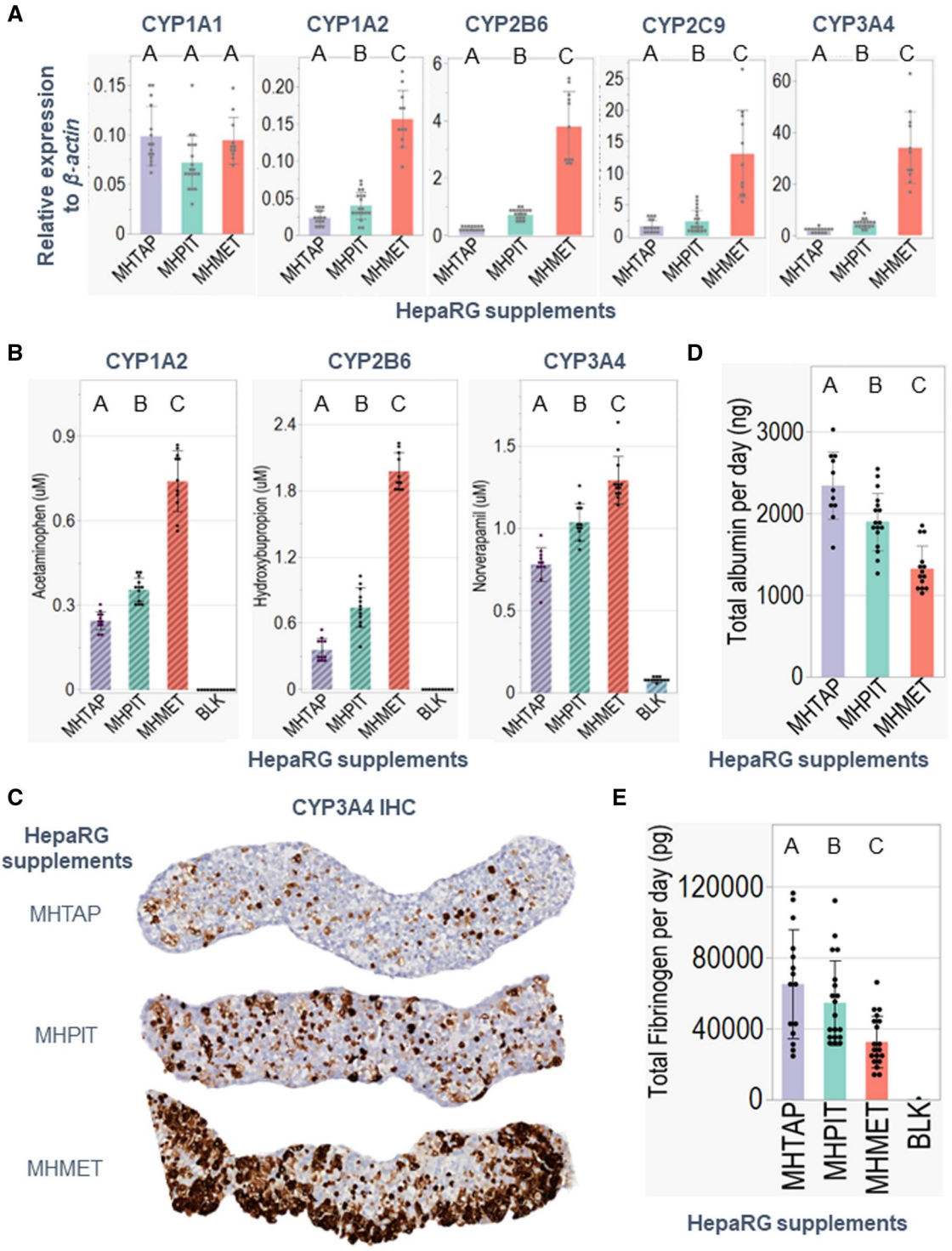

Figure 5. HepaRG microtissues can recapitulate an *in vivo*-like zonation of nitrogen and xenobiotic metabolisms by maturing in medium supplements with varying amounts of DMSO. Gene expression relative to housekeeping gene β-actin (A). Metabolic function of hepatic Phase I CYP enzymes (B), CYP3A4 protein expression by immunohistochemistry (C). Levels of human albumin (D) and fibrinogen (E) protein synthesis by ELISA. HepaRG 3D microtissues were matured in the ring trough for 10 days in MHTAP, MHPIT, or MHMET medium. CYP1A2, CYP2B6, and CYP3A4 function was evaluated by incubating HepaRG 3D microtissues with phenacetin (125 μM for 24 h), bupropion (100 μM for 24 h), verapamil (20 μM for 24 h), respectively. HepaRG microtissues were formalin-fixed, paraffin-embedded, and sectioned for immunostaining analyses. Data = mean ± SD. One-way ANOVA with *post hoc* Tukey HSD test, or their nonparametric equivalent, were used to examine statistical significance between maturation days. Bars that do not share the same letters are significantly different (p value $\leq .05$).

diffusion throughout the well is required. To address this property of the platform, human albumin (Figs. 6A and 6B) or phenacetin (Figs. 6C and 6D) spiked medium was incubated in wells with or without agarose in identical final concentrations for 24 h. No alteration of medium albumin or phenacetin concentration was observed. Furthermore, to test the diffusivity of compounds

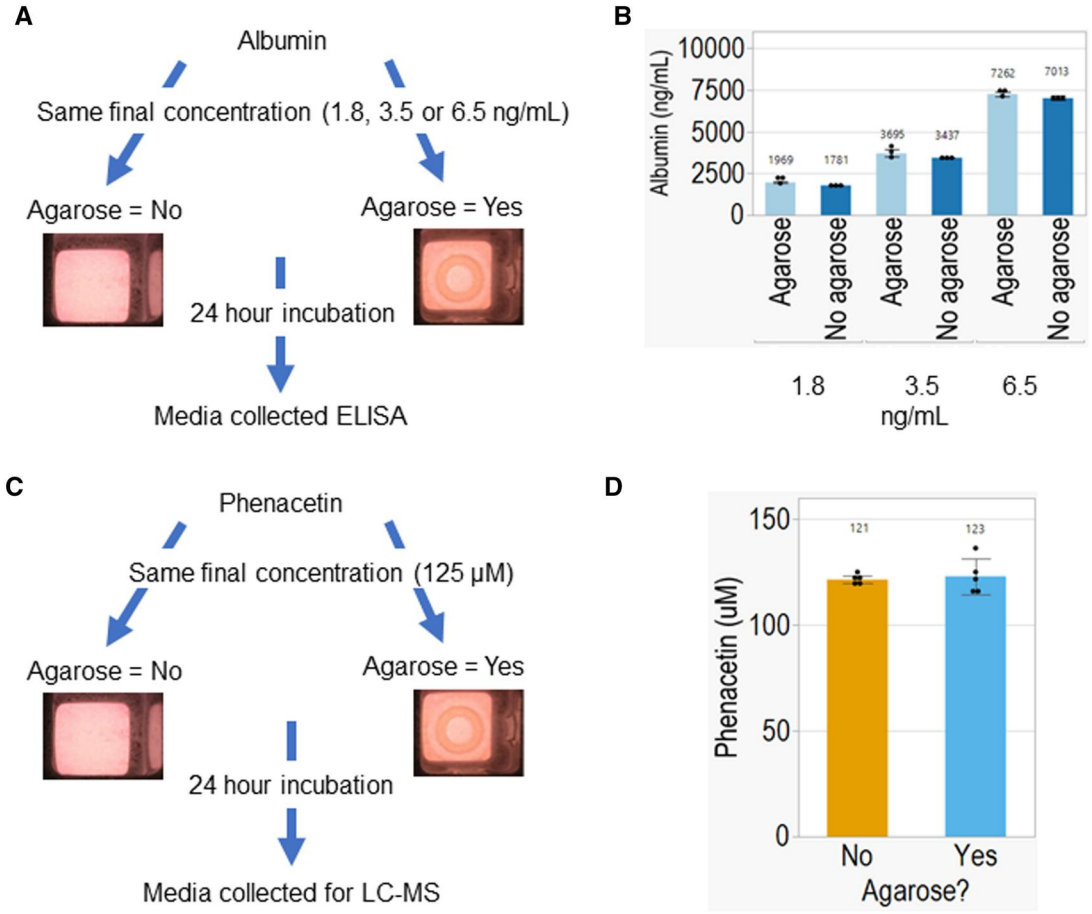

Figure 6. The agarose mold did not alter medium constituent concentration. A, Diagram of the experimental design for examining whether agarose alters albumin concentration. B, Albumin concentrations with or without agarose in the platform are comparable after 24 h of incubation with albumin-spiked medium at 3 different final concentrations. C, Experimental design for examining whether agarose alters phenacetin concentration. D, Phenacetin concentrations of wells with or without the agarose in the platform were similar after 24 h of incubation with phenacetin-spiked medium at a final concentration of 125 µM.

in the platform, HepaRG microtissues were incubated in medium with phenacetin (final concentration at 125 µM) for 1, 4, or 24 h, and the acetaminophen medium concentration in the top layer of the well was compared with that of the whole well (Figure 7A). Regardless of medium collection method, medium acetaminophen (Figure 7B) concentrations were comparable for each of the 3 incubation times.

HepaRG 3D microtissue metabolized testosterone and reduced testosterone-mediated activation of androgen receptor

To demonstrate the efficacy of this 2-chamber coculture model in testing drug/chemical toxicity on target tissues with human liver metabolism, we executed a proof-of-concept experiment by coculturing HepaRG 3D microtissues that were matured for 10 days with AR-CALUX reporter cells as the target to investigate the effects of human liver metabolism on testosterone (T) (Figure 8A), and the associated activation of AR. We cocultured the 10-day matured HepaRG microtissues with AR-CALUX for 24 h in the absence or presence of testosterone at 4 different physiologically relevant doses (10, 30, 100, or 1000 nM). Our coculture data showed that HepaRG 3D microtissues significantly reduced activation of AR-CALUX cells at all doses of T examined (Figure 8B). LC-MS/MS analysis of the cocultured media showed that the presence of HepaRG microtissues significantly reduced media testosterone concentrations at all 4 doses of testosterone (Figure 8C, top). The percentage of testosterone being metabolized by HepaRG microtissues was approximately 50% of the starting testosterone doses (Figure 8C, bottom). Correspondingly, the presence of HepaRG microtissues significantly increased media androstenedione concentrations to approximately 17% of the starting testosterone doses (Figure 8D). The AR-CALUX luminescence had a linear relationship to the log of the testosterone media concentrations without HepaRGs as determined by LC-MS/MS ($R^2 = 0.9401$). 6β-hydroxytestosterone was below the limit of detection of 5 nM for all testosterone doses tested. Dihydrotestosterone was not produced in measurable amounts by HepaRG microtissues. We observed the potential presence of testosterone glucuronide in our LC-MS/MS chromatograms (Supplementary Figure 3).

Discussion

Chemicals and drugs can undergo metabolism in hepatic and peripheral tissues and generate metabolites with altered activities and toxicities on biological targets as compared with their parent compounds. Therefore, adding human metabolic capabilities to *in vitro* assays is an important need to decrease uncertainty as new approach methodologies are developed for regulatory decision making.

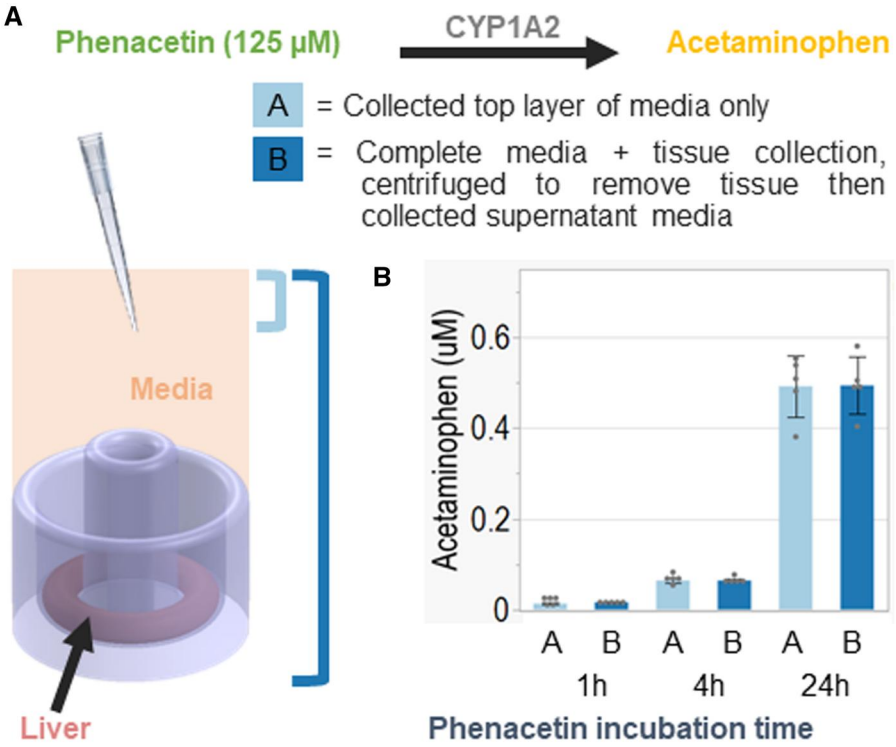

Figure 7. Agarose did not alter the diffusion of compounds. A, Experimental design for examining the diffusivity of acetaminophen in the 2-chamber platform. B, Acetaminophen concentrations of the top layer of medium are identical to the concentration of the whole well after HepaRG 3D microtissues are incubated in phenacetin-spiked medium at a final concentration of 125 μM for 1, 4, or 24 .

To address this need, we engineered a 2-chamber liver-organ coculture model in a higher-throughput 96-well format for the determination of toxicity on target tissues in the presence of human liver biology and metabolism. This system made of 2% agarose hydrogel consists of a ring-shaped outer trough for culturing human liver cells in 3D surrounding a center well for culturing the biological target of choice. We introduced hepatic metabolic capacity by culturing human hepatoma HepaRG cells (Gripon *et al.*, 2002) as 3D microtissues in contrast to other coculture systems with hepatic metabolism for the following reasons: (1) to overcome the limitations of using PHH (Chao *et al.*, 2009; Godoy *et al.*, 2013; Jackson *et al.*, 2016; Mitaka, 1998; Nyberg *et al.*, 1994; Ozawa *et al.*, 2000; Parkinson, 1996) and liver slices (Miller *et al.*, 1993; Vickers *et al.*, 1992), including donor-to-donor variability (Ozawa *et al.*, 2000; Parkinson, 1996), and the rapid de-differentiation of PHH cultured in suspension (Jackson *et al.*, 2016); (2) to better recapitulate liver biology than using liver-derived or genetically engineered cell lines expressing biotransformation enzymes (Bull *et al.*, 2001; Clarke, 1998; Hashizume *et al.*, 2009; Schmalix *et al.*, 1996) and subcellular fractions (eg, S9) (Bimboes and Greim, 1976; Charles *et al.*, 2000; Cox *et al.*, 2016; Taxvig *et al.*, 2011; van Vugt-Lussenburg *et al.*, 2018); (3) 3D HepaRG has improved metabolic function over 2D HepaRG culture (Ramaiahgari *et al.*, 2017) with stable hepatic phenotypes (eg, liver enzyme induction, albumin production, and biliary excretion) lasting up to 60 days (Ramaiahgari *et al.*, 2017; Takahashi *et al.*, 2015; Yokoyama *et al.*, 2018), and (4) HepaRG microtissues can represent both Phase I and II of hepatic metabolism in long-term culture, thus overcoming the limitations of S9 done without Phase II cofactors that can potentially increase false-positive outcomes of parent compounds by exacerbating the effects of reactive intermediates generated by Phase I oxidation alone, and its short metabolic activities of up to 2 h (Bimboes and Greim, 1976; Cox *et al.*, 2016; Taxvig *et al.*, 2011).

Our 3D HepaRG microtissues had robust protein expression of liver biomarkers (albumin, ASGR2, CYP3A4, MRP2, and glycogen), exhibited ultrastructure of bile canaliculi with microvilli, tight junctions, and abundant mitochondria that illustrated the functional maturity of these human hepatocytes. Importantly, 3D HepaRG microtissues displayed hepatic Phase I/II metabolism over the course of 17 days that plateaus at day 10. Interestingly, our liver tissues exhibited hepatic zonation metabolic characteristics by maturing the tissues in different HepaRG medium supplements. Mature mammalian liver displays metabolic zonation within the hepatic microcirculatory unit called the acinus (Lindros, 1997; Oinonen and Lindros, 1998; Torre *et al.*, 2010). The periportal zone exhibits greater general metabolism including oxidative energy metabolism, gluconeogenesis, fatty acid oxidation, and cholesterol synthesis, whereas the perivenous zone has higher Phase I xenobiotic metabolism (Lindros, 1997; Oinonen and Lindros, 1998; Torre *et al.*, 2010). Despite not capturing the oxygen tension changes across the liver zones, our method of modulating HepaRG microtissue zonation may ease the challenges in elucidating how environmental agents can impact hepatic zonal metabolism, hepatoxicity, and their effects on target tissues using *in vitro* systems (Ahn *et al.*, 2019; Gough *et al.*, 2021; Kang *et al.*, 2018; Ma *et al.*, 2020; McEnerney *et al.*, 2017; Scheidecker *et al.*, 2020; Wahlicht *et al.*, 2020).

The integration of liver metabolism with targets could be accomplished by different techniques including (1) the transferring of chemical-spiked medium that was preincubated with hepatocytes to targets; (2) coculture techniques (eg, microsomal fractions with target cells, transwell, organ-on-a-chip) (Li *et al.*, 2012, 2016; Mollergues *et al.*, 2017); and (3) genetically engineered cells that act simultaneously as both indicators of toxicity and

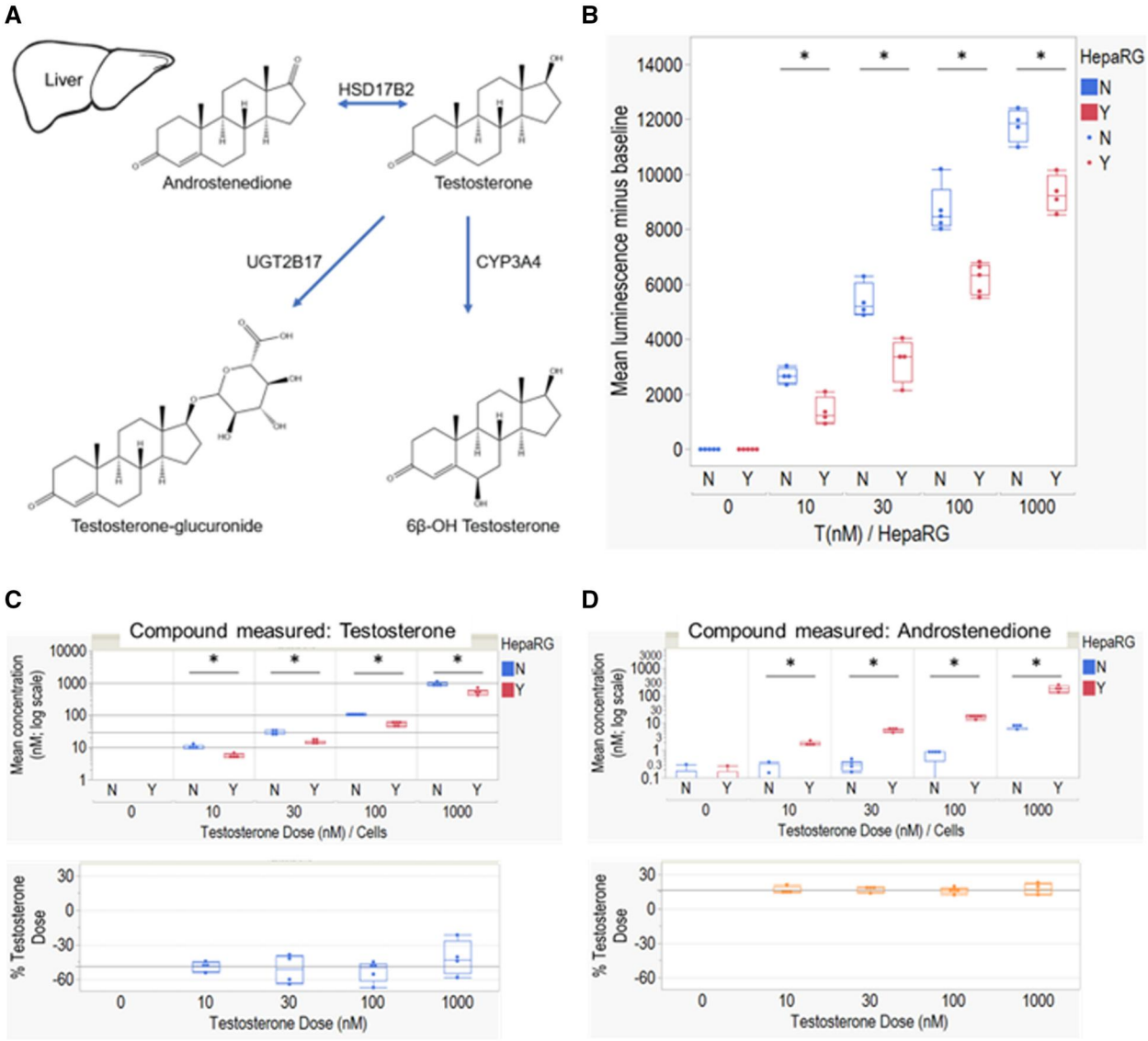

Figure 8. HepaRG 3D microtissues metabolized testosterone and reduced testosterone-mediated activation of androgen receptor (AR). Simplified metabolic pathway of testosterone biotransformation in the liver (A). Mean luminescence minus baseline of AR-CALUX reporter cells cocultured with or without HepaRG 3D microtissues after incubation with testosterone (T) at 0, 10, 30, 100, or 1000 nM for 24 h (B). Mean media testosterone concentration in nM (top) of wells with or without HepaRG 3D microtissues after incubation with testosterone (T) at 0, 10, 30, 100, or 1000 nM for 24 h, and as % of starting testosterone doses (bottom) in wells with HepaRG (C). Mean media androstenedione concentration in nM (top) of wells with or without HepaRG 3D microtissues after incubation with testosterone (T) at 0, 10, 30, 100, or 1000 nM for 24 h, and as % of starting testosterone doses (bottom) of wells with HepaRG (D). Data = mean ± SD. Student's t test was used to examine statistical significance for the effects of HepaRG on AR-CALUX activation and compounds in media measured by LC-MS for each of the 4 doses independently. * $p < .05$. CYP3A4, cytochrome P450 family 3 member A4; HSD17B2, 17β-hydroxysteroid dehydrogenase 2; UGT2B17, UDP glucuronosyltransferase family 2 member B17.

the source of metabolism (Bull *et al.*, 2001; Schmalix *et al.*, 1996). The recently developed ToxCast/Tox21 HTS program introduced hepatic metabolism by using encapsulated rat hepatic S9 fractions in alginate microspheres attached to 96-well peg lids with an NRS cocktail that supported Phase I xenobiotic metabolism while minimizing cytotoxicity (Bimboes and Greim, 1976; Cox *et al.*, 2016).

Our 2-chamber coculture system aims to better recapitulate the physiological process of how chemicals interact with target tissue in the presence of hepatic metabolism than existing systems. Chemicals that are delivered to the human liver undergo a combination of Phase I/II metabolism that are compound-specific to generate a spectrum of metabolites. Selected molecules then exit the hepatocytes into the systemic circulation, whereas others remain in the hepatocytes or exit via bile canaliculi (Doehmer, 2006; Jacobs *et al.*, 2008). The molecules that enter the systemic circulation travel to extrahepatic tissues and elicit their effects. Our platform with 2% agarose hydrogel allows for the liver and the target cells to be cultured separately with no direct physical contact while maintaining rapid and efficient diffusion of medium and chemicals throughout the entire well, thus appropriately mimicking the physiological transport of chemicals between liver and target tissues. Other advantages of using agarose hydrogel includes: (1) nonadhesive to cells, thus allowing seeded cells to form 3D tissues (Dean *et al.*, 2007; Ip *et al.*, 2018, 2022; Leary *et al.*, 2018); (2) remains inert to chemicals tested, a significant advantage over other materials (eg, PDMS in organ-on-chips) in existing coculture systems that are known to

interfere with drug response bioassays though chemical adsorption (van Meer *et al.*, 2017); (3) hydrogel transparency allows for efficient imaging with widefield and confocal microscopy (Leary *et al.*, 2018); and for immunohistochemical analyses *in situ* (Boutin *et al.*, 2018; 2022), (4) agarose system design can be altered by modifying the master metal mold, allowing the platform to be scalable.

We developed 2 versions where the targets can either be cultured in 3D or as a 2D monolayer of cells, to better suit the biological context of the assay. For most target tissues, cells cultured as 3D microtissues better recapitulate the biology of the target organ (Ip *et al.*, 2022). The 2D target cell option is applicable for reporter cell lines such as CALUX cells (Chemically Activated LUciferase gene eXpression, BioDetection Systems, Amsterdam, The Netherlands) (Mollergues *et al.*, 2017; Murk *et al.*, 1996), to elucidate the response element activation capacities of parent compounds in the presence of human hepatic biotransformation. By coculturing 3D HepaRG with AR-CALUX cells, our proof-of-concept study illustrated the efficacy of this coculture model in evaluating testosterone-mediated AR responses in the presence of human liver metabolism at physiologically relevant testosterone doses (10–1000 nM). After 24 h at all doses, half of the testosterone was metabolized in the presence of 3D HepaRG, which corresponded to 17% conversion to androstenedione. These results suggested a linear, nonsaturating conversion of testosterone to androstenedione at physiologically relevant doses. The metabolism of testosterone resulted in a predictable decrease in AR activation, given the relative androgenicity of testosterone versus androstenedione (Sonneveld *et al.*, 2005). Comparing the early model-development work and the proof-of-concept coculture study illustrated the dose-dependent metabolism of testosterone, where 6β-hydroxytestosterone was detected only with the nonphysiologically high testosterone concentration of 200 μM (Figure 4D).

Similar to other plate-based coculture systems, ours is a closed system without excretion as a route of elimination. Our "route of elimination" is the formation of unmeasured metabolites from a pool of continuously active equilibrium reactions. It has also been shown that major glucuronide metabolites are transported by the enzyme MRP2 in the liver (Li *et al.*, 2019), and MRP2 is functional within HepaRG 3D microtissues (Ramaiahgari *et al.*, 2017). Our immunohistochemical staining showed that MRP2 was expressed predominantly in the interior of the 3D HepaRG microtissues. Thus, it is plausible that these metabolites were trapped within the microtissues instead of being released into the media.

Some of the limitations of this coculture system include the complexity of fabricating and utilizing this model, which can be alleviated with automation. Automation would also reduce the variability that is introduced by manual pipetting during cell seeding and media exchanges. The suboptimal recapitulation of human hepatic metabolism by 3D HepaRG can be overcome by utilizing more advanced human liver organoids that are currently under development (Liu *et al.*, 2022).

In summary, this 2-chamber agarose system introduces human-relevant liver xenobiotic metabolic capabilities into higher-throughput toxicology screening with different target tissues and repeat dosing capability. Future experiments will explore: (1) multiple time points, measuring additional metabolites in media and in the liver microtissues to provide insight into the kinetics of the coculture system; (2) modifications of mold design to increase the number of HepaRG cells/well; (3) the enzyme induction capacities; (4) longer-term stability of the 3D HepaRG microtissues for use in repeated exposure experimental designs; and (5) modeling methods for *in vitro* to *in vivo* extrapolation of the results.

Supplementary data

Supplementary data are available at *Toxicological Sciences* online.

Declaration of conflicting interests

The authors declare that the research was conducted in the absence of any commercial or financial relationships that could be construed as a potential conflict of interest. B.C.I., H.L., S.J.H., J.R.M., and K.B. are joint inventors of the provisional patent that describe the invention of the multicompartment device described in this manuscript. J.R.M. has an equity interest in Microtissues, Inc. and in XM Therapeutics, Inc. These relationships have been reviewed and are managed by Brown University in accordance with its conflict of interest policies.

Acknowledgments

We thank Donna McGraw Weiss ('89) and Jason Weiss for their generous support to the Center for Alternatives to Animals in Testing at Brown University. We also thank the Brown University Molecular Pathology Core, the Brown University Genomics Core, and the Leduc Bioimaging Facility for their support.

Funding

The National Institutes of Health - The National Institute of Environmental Health Sciences (U01 ES028184); Unilever, UK; the Center for Alternatives to Animals in Testing at Brown University.

References

Ahn, J., Ahn, J. H., Yoon, S., Nam, Y. S., Son, M. Y., and Oh, J. H. (2019). Human three-dimensional in vitro model of hepatic zonation to predict zonal hepatotoxicity. *J. Biol. Eng.* **13**, 22.

Bimboes, D., and Greim, H. (1976). Human lymphocytes as target cells in a metabolizing test system in vitro for detecting potential mutagens. *Mutat. Res.* **35**, 155–160.

Boutin, M. E., Strong, C. E., Van Hese, B., Hu, X., Itkin, Z., Chen, Y. C., LaCroix, A., Gordon, R., Guicherit, O., Carromeu, C., *et al.* (2022). A multiparametric calcium signal screening platform using iPSC-derived cortical neural spheroids. *SLAS Discov.* **27**, 209–218.

Boutin, M. E., Voss, T. C., Titus, S. A., Cruz-Gutierrez, K., Michael, S., and Ferrer, M. (2018). A high-throughput imaging and nuclear segmentation analysis protocol for cleared 3D culture models. *Sci. Rep.* **8**, 11135.

Bull, S., Langezaal, I., Clothier, R., and Coecke, S. (2001). A genetically engineered cell-based system for detecting metabolism-mediated toxicity. *Altern. Lab. Anim.* **29**, 703–716.

Chao, P., Maguire, T., Novik, E., Cheng, K. C., and Yarmush, M. L. (2009). Evaluation of a microfluidic based cell culture platform with primary human hepatocytes for the prediction of hepatic clearance in human. *Biochem. Pharmacol.* **78**, 625–632.

Charles, G. D., Bartels, M. J., Gennings, C., Zacharewski, T. R., Freshour, N. L., Bhaskar Gollapudi, B., and Carney, E. W. (2000). Incorporation of S-9 activation into an ER-alpha transactivation assay. *Reprod. Toxicol.* **14**, 207–216.

Chen, Y., Liu, L., Monshouwer, M., and Fretland, A. J. (2011). Determination of time-dependent inactivation of CYP3A4 in cryopreserved human hepatocytes and assessment of human drug-drug interactions. *Drug Metab. Dispos.* **39**, 2085–2092.

Clarke, S. E. (1998). In vitro assessment of human cytochrome P450. *Xenobiotica* **28**, 1167–1202.

Cox, J. A., Fellows, M. D., Hashizume, T., and White, P. A. (2016). The utility of metabolic activation mixtures containing human hepatic post-mitochondrial supernatant (S9) for in vitro genetic toxicity assessment. *Mutagenesis* **31**, 117–130.

Dean, D. M., Napolitano, A. P., Youssef, J., and Morgan, J. R. (2007). Rods, tori, and honeycombs: The directed self-assembly of microtissues with prescribed microscale geometries. *Faseb J.* **21**, 4005–4012.

Deisenroth, C., DeGroot, D. E., Zurlinden, T., Eicher, A., McCord, J., Lee, M. Y., Carmichael, P., and Thomas, R. S. (2020). The Alginate Immobilization of Metabolic Enzymes platform retrofits an estrogen receptor transactivation assay with metabolic competence. *Toxicol. Sci.* **178**, 281–301.

Doehmer, J. (2006). Predicting drug metabolism-dependent toxicity for humans with a genetically engineered cell battery. *Altern. Lab. Anim.* **34**, 561–575.

FDA. (2018). *Bioanalytical Method Validation—Guidance for Industry*. HHS US. Available at: https://www.fda.gov/files/drugs/published/Bioanalytical-Method-Validation-Guidance-for-Industry.pdf

Franco, O. E., Jiang, M., Strand, D. W., Peacock, J., Fernandez, S., Jackson, R. S., 2nd, Revelo, M. P., Bhowmick, N. A., and Hayward, S. W. (2011). Altered TGF-β signaling in a subpopulation of human stromal cells promotes prostatic carcinogenesis. *Cancer Res.* **71**, 1272–1281.

Godoy, P., Hewitt, N. J., Albrecht, U., Andersen, M. E., Ansari, N., Bhattacharya, S., Bode, J. G., Bolleyn, J., Borner, C., Böttger, J., *et al.* (2013). Recent advances in 2D and 3D in vitro systems using primary hepatocytes, alternative hepatocyte sources and non-parenchymal liver cells and their use in investigating mechanisms of hepatotoxicity, cell signaling and ADME. *Arch. Toxicol.* **87**, 1315–1530.

Gough, A., Soto-Gutierrez, A., Vernetti, L., Ebrahimkhani, M. R., Stern, A. M., and Taylor, D. L. (2021). Human biomimetic liver microphysiology systems in drug development and precision medicine. *Nat. Rev. Gastroenterol. Hepatol.* **18**, 252–268.

Gripon, P., Rumin, S., Urban, S., Le Seyec, J., Glaise, D., Cannie, I., Guyomard, C., Lucas, J., Trepo, C., and Guguen-Guillouzo, C. (2002). Infection of a human hepatoma cell line by hepatitis B virus. *Proc. Natl. Acad. Sci. U.S.A.* **99**, 15655–15660.

Gunness, P., Mueller, D., Shevchenko, V., Heinzle, E., Ingelman-Sundberg, M., and Noor, F. (2013). 3d organotypic cultures of human HepaRG cells: A tool for in vitro toxicity studies. *Toxicol. Sci.* **133**, 67–78.

Hanke, N., Türk, D., Selzer, D., Wiebe, S., Fernandez, É., Stopfer, P., Nock, V., and Lehr, T. (2020). A mechanistic, enantioselective, physiologically based pharmacokinetic model of verapamil and norverapamil, built and evaluated for drug-drug interaction studies. *Pharmaceutics* **12**, 556.

Hashizume, T., Yoshitomi, S., Asahi, S., Matsumura, S., Chatani, F., and Oda, H. (2009). In vitro micronucleus test in HepG2 transformants expressing a series of human cytochrome P450 isoforms with chemicals requiring metabolic activation. *Mutat. Res.* **677**, 1–7.

Hoekstra, R., Nibourg, G. A., van der Hoeven, T. V., Plomer, G., Seppen, J., Ackermans, M. T., Camus, S., Kulik, W., van Gulik, T. M., Elferink, R. P., *et al.* (2013). Phase 1 and phase 2 drug metabolism and bile acid production of HepaRG cells in a bioartificial liver in absence of dimethyl sulfoxide. *Drug Metab. Dispos.* **41**, 562–567.

ICH. (2022). *Bioanalytical Method Validation and Study Sample Analysis M10*. ICH. Available at: https://database.ich.org/sites/default/files/M10_Guideline_Step4_2022_0524.pdf

Ip, B. C., Cui, F., Wilks, B. T., Murphy, I. J., Tripathi, A., and Morgan, J. R. (2018). Perfused organ cell-dense macrotissues assembled from prefabricated living microtissues. *Adv. Biosys.* **2**, 1800076.

Ip, B. C., Leary, E., Knorlein, B., Reich, D., Van, V., Manning, J., and Morgan, J. R. (2022). 3D microtissues mimic the architecture, estradiol synthesis and gap junction intercellular communication of the avascular granulosa. *Toxicol. Sci.* **186**, 29–42.

Jackson, J. P., Li, L., Chamberlain, E. D., Wang, H., and Ferguson, S. S. (2016). Contextualizing hepatocyte functionality of cryopreserved HepaRG cell cultures. *Drug Metab. Dispos.* **44**, 1463–1479.

Jacobs, M. N., Janssens, W., Bernauer, U., Brandon, E., Coecke, S., Combes, R., Edwards, P., Freidig, A., Freyberger, A., Kolanczyk, R., *et al.* (2008). The use of metabolising systems for in vitro testing of endocrine disruptors. *Curr. Drug Metab.* **9**, 796–826.

Kang, Y. B. A., Eo, J., Mert, S., Yarmush, M. L., and Usta, O. B. (2018). Metabolic patterning on a chip: Towards in vitro liver zonation of primary rat and human hepatocytes. *Sci. Rep.* **8**, 8951.

Leary, E., Rhee, C., Wilks, B. T., and Morgan, J. R. (2018). Quantitative live-cell confocal imaging of 3D spheroids in a high-throughput format. *SLAS Technol.* **23**, 231–242.

Leite, S. B., Wilk-Zasadna, I., Zaldivar, J. M., Airola, E., Reis-Fernandes, M. A., Mennecozzi, M., Guguen-Guillouzo, C., Chesne, C., Guillou, C., Alves, P. M., *et al.* (2012). Three-dimensional HepaRG model as an attractive tool for toxicity testing. *Toxicol. Sci.* **130**, 106–116.

Li, A. P., Uzgare, A., and LaForge, Y. S. (2012). Definition of metabolism-dependent xenobiotic toxicity with co-cultures of human hepatocytes and mouse 3T3 fibroblasts in the novel integrated discrete multiple organ co-culture (IdMOC) experimental system: Results with model toxicants aflatoxin B1, cyclophosphamide and tamoxifen. *Chem. Biol. Interact.* **199**, 1–8.

Li, C. Y., Basit, A., Gupta, A., Gáborik, Z., Kis, E., and Prasad, B. (2019). Major glucuronide metabolites of testosterone are primarily transported by MRP2 and MRP3 in human liver, intestine and kidney. *J. Steroid Biochem. Mol. Biol.* **191**, 105350.

Li, Z., Guo, Y., Yu, Y., Xu, C., Xu, H., and Qin, J. (2016). Assessment of metabolism-dependent drug efficacy and toxicity on a multilayer organs-on-a-chip. *Integr Biol (Camb)* **8**, 1022–1029.

Lindros, K. O. (1997). Zonation of cytochrome p450 expression, drug metabolism and toxicity in liver. *Gen. Pharmacol.* **28**, 191–196.

Liu, Q., Zeng, A., Liu, Z., Wu, C., and Song, L. (2022). Liver organoids: From fabrication to application in liver diseases. *Front. Physiol.* **13**, 956244.

Lundberg, P., and Kuchel, P. W. (1997). Diffusion of solutes in agarose and alginate gels: 1H and 23Na PFGSE and 23Na TQF NMR studies. *Magn. Reson. Med.* **37**, 44–52.

Ma, R., Martínez-Ramírez, A. S., Borders, T. L., Gao, F., and Sosa-Pineda, B. (2020). Metabolic and non-metabolic liver zonation is established non-synchronously and requires sinusoidal Wnts. *Elife.* **9**, e46206.

McEnerney, L., Duncan, K., Bang, B. R., Elmasry, S., Li, M., Miki, T., Ramakrishnan, S. K., Shah, Y. M., and Saito, T. (2017). Dual modulation of human hepatic zonation via canonical and non-canonical Wnt pathways. *Exp. Mol. Med.* **49**, e413.

Miller, M. G., Beyer, J., Hall, G. L., deGraffenried, L. A., and Adams, P. E. (1993). Predictive value of liver slices for metabolism and

toxicity in vivo: Use of acetaminophen as a model hepatotoxicant. *Toxicol. Appl. Pharmacol.* **122**, 108–116.

Mitaka, T. (1998). The current status of primary hepatocyte culture. *Int. J. Exp. Pathol.* **79**, 393–409.

Mollergues, J., van Vugt-Lussenburg, B., Kirchnawy, C., Bandi, R. A., van der Lee, R. B., Marin-Kuan, M., Schilter, B., and Fussell, K. C. (2017). Incorporation of a metabolizing system in biodetection assays for endocrine active substances. *Altex* **34**, 389–398.

Murk, A. J., Legler, J., Denison, M. S., Giesy, J. P., van de Guchte, C., and Brouwer, A. (1996). Chemical-activated luciferase gene expression (CALUX): A novel in vitro bioassay for Ah receptor active compounds in sediments and pore water. *Fundam. Appl. Toxicol.* **33**, 149–160.

Nyberg, S. L., Remmel, R. P., Mann, H. J., Peshwa, M. V., Hu, W.-S., and Cerra, F. B. (1994). Primary hepatocytes outperform HepG2 cells as the source of biotransformation functions in a bioartificial liver. *Ann. Surg.* **220**, 59.

Oinonen, T., and Lindros, K. O. (1998). Zonation of hepatic cytochrome P-450 expression and regulation. *Biochem. J.* **329**(Pt 1), 17–35.

Ozawa, S., Ohta, K., Miyajima, A., Kurebayashi, H., Sunouchi, M., Shimizu, M., Murayama, N., Matsumoto, Y., Fukuoka, M., and Ohno, Y. (2000). Metabolic activation of o-phenylphenol to a major cytotoxic metabolite, phenylhydroquinone: Role of human CYP1A2 and rat CYP2C11/CYP2E1. *Xenobiotica* **30**, 1005–1017.

Parkinson, A. (1996). An overview of current cytochrome P450 technology for assessing the safety and efficacy of new materials. *Toxicol. Pathol.* **24**, 48–57.

Pelkonen, O., Turpeinen, M., Hakkola, J., Honkakoski, P., Hukkanen, J., and Raunio, H. (2008). Inhibition and induction of human cytochrome P450 enzymes: Current status. *Arch. Toxicol.* **82**, 667–715.

Ramaiahgari, S. C., Waidyanatha, S., Dixon, D., DeVito, M. J., Paules, R. S., and Ferguson, S. S. (2017). Three-dimensional (3D) HepaRG spheroid model with physiologically relevant xenobiotic metabolism competence and hepatocyte functionality for liver toxicity screening. *Toxicol. Sci.* **160**, 189–190.

Scheidecker, B., Shinohara, M., Sugimoto, M., Danoy, M., Nishikawa, M., and Sakai, Y. (2020). Induction of in vitro metabolic zonation in primary hepatocytes requires both near-physiological oxygen concentration and flux. *Front. Bioeng. Biotechnol.* **8**, 524.

Schmalix, W. A., Lang, D., Schneider, A., Bocker, R., Greim, H., and Doehmer, J. (1996). Stable expression and coexpression of human cytochrome P450 oxidoreductase and cytochrome P450 1A2 in V79 Chinese hamster cells: Sensitivity to quinones and biotransformation of 7-alkoxyresorufins and triazines. *Drug Metab. Dispos.* **24**, 1314–1319.

Smith, C. M., Nolan, C. K., Edwards, M. A., Hatfield, J. B., Stewart, T. W., Ferguson, S. S., Lecluyse, E. L., and Sahi, J. (2012). A comprehensive evaluation of metabolic activity and intrinsic clearance in suspensions and monolayer cultures of cryopreserved primary human hepatocytes. *J. Pharm. Sci.* **101**, 3989–4002.

Sonneveld, E., Jansen, H. J., Riteco, J. A., Brouwer, A., and van der Burg, B. (2005). Development of androgen- and estrogen-responsive bioassays, members of a panel of human cell line-based highly selective steroid-responsive bioassays. *Toxicol. Sci.* **83**, 136–148.

Sudo, M., Nishihara, M., Takahashi, J., and Asahi, S. (2017). Long-term stability of cryopreserved human hepatocytes: Evaluation of phase I and II drug-metabolizing enzyme activities and CYP3A4/5 induction for more than a decade. *Drug Metab. Dispos.* **45**, 734–736.

Takahashi, Y., Hori, Y., Yamamoto, T., Urashima, T., Ohara, Y., and Tanaka, H. (2015). Three-dimensional (3D) spheroid cultures improve the metabolic gene expression profiles of HepaRG cells. *Biosci Rep* **35**, e00208.

Taxvig, C., Olesen, P. T., and Nellemann, C. (2011). Use of external metabolizing systems when testing for endocrine disruption in the T-screen assay. *Toxicol. Appl. Pharmacol.* **250**, 263–269.

Torre, C., Perret, C., and Colnot, S. (2010). Molecular determinants of liver zonation. *Prog. Mol. Biol. Transl. Sci.* **97**, 127–150.

Tracy, T. S., Korzekwa, K. R., Gonzalez, F. J., and Wainer, I. W. (1999). Cytochrome P450 isoforms involved in metabolism of the enantiomers of verapamil and norverapamil. *Br. J. Clin. Pharmacol.* **47**, 545–552.

Turpeinen, M., Tolonen, A., Chesne, C., Guillouzo, A., Uusitalo, J., and Pelkonen, O. (2009). Functional expression, inhibition and induction of CYP enzymes in HepaRG cells. *Toxicol. In Vitro* **23**, 748–753.

van der Burg, B., Winter, R., Man, H-y., Vangenechten, C., Berckmans, P., Weimer, M., Witters, H., and van der Linden, S. (2010). Optimization and prevalidation of the in vitro AR CALUX method to test androgenic and antiandrogenic activity of compounds. *Reprod. Toxicol.* **30**, 18–24.

van Meer, B. J., de Vries, H., Firth, K. S. A., van Weerd, J., Tertoolen, L. G. J., Karperien, H. B. J., Jonkheijm, P., Denning, C., IJzerman, A. P., and Mummery, C. L. (2017). Small molecule absorption by PDMS in the context of drug response bioassays. *Biochem. Biophys. Res. Commun.* **482**, 323–328.

van Vugt-Lussenburg, B. M. A., van der Lee, R. B., Man, H. Y., Middelhof, I., Brouwer, A., Besselink, H., and van der Burg, B. (2018). Incorporation of metabolic enzymes to improve predictivity of reporter gene assay results for estrogenic and antiandrogenic activity. *Reprod. Toxicol.* **75**, 40–48.

VandenBrink, B. M., and Isoherranen, N. (2010). The role of metabolites in predicting drug-drug interactions: Focus on irreversible cytochrome P450 inhibition. *Curr. Opin. Drug Discov. Dev.* **13**, 66–77.

Vickers, A. E., Fischer, V., Connors, S., Fisher, R. L., Baldeck, J. P., Maurer, G., and Brendel, K. (1992). Cyclosporin a metabolism in human liver, kidney, and intestine slices. Comparison to rat and dog slices and human cell lines. *Drug Metab. Dispos.* **20**, 802–809.

Wahlicht, T., Vièyres, G., Bruns, S. A., Meumann, N., Büning, H., Hauser, H., Schmitz, I., Pietschmann, T., and Wirth, D. (2020). Controlled functional zonation of hepatocytes in vitro by engineering of Wnt signaling. *ACS Synth. Biol.* **9**, 1638–1649.

Yeo, K. R., and Yeo, W. W. (2001). Inhibitory effects of verapamil and diltiazem on simvastatin metabolism in human liver microsomes. *Br. J. Clin. Pharmacol.* **51**, 461–470.

Yokoyama, Y., Sasaki, Y., Terasaki, N., Kawataki, T., Takekawa, K., Iwase, Y., Shimizu, T., Sanoh, S., and Ohta, S. (2018). Comparison of drug metabolism and its related hepatotoxic effects in heparg, cryopreserved human hepatocytes, and HepG2 cell cultures. *Biol. Pharm. Bull.* **41**, 722–732.